SIAM J. SCI. COMPUT.
Vol. 40, No. 2, pp. B637–B662

COUPLING OF DISCONTINUOUS GALERKIN SCHEMES FOR VISCOUS FLOW IN POROUS MEDIA WITH ADSORPTION*

RAIMUND BÜRGER†, SUDARSHAN KUMAR KENETTINKARA‡, RICARDO RUIZ BAIER§, AND HECTOR TORRES¶

Abstract. Polymer flooding is an important stage of enhanced oil recovery in petroleum reservoir engineering. A model of this process is based on the study of multicomponent viscous flow in porous media with adsorption. This model can be expressed as a Brinkman-based model of flow in porous media coupled to a nonstrictly hyperbolic system of conservation laws for multiple components (water and polymers) that form the aqueous phase. The discretization proposed for this coupled flow-transport problem combines an **H**(div)-conforming discontinuous Galerkin (DG) method for the Brinkman flow problem with a classical DG method for the transport equations. The DG formulation of the transport problem is based on discontinuous numerical fluxes. An invariant region property is proved under the (mild) assumption that the underlying mesh is a **B**-triangulation [B. Cockburn, S. Hou, and C.-W. Shu, *Math. Comp.*, 54 (1990), pp. 545–581]. This property states that only physically relevant (bounded and nonnegative) saturation and concentration values are generated by the scheme. Numerical tests illustrate the accuracy and stability of the proposed method.

Key words. multicomponent viscous flow in porous media, coupled flow-transport problem, discontinuous Galerkin method, invariant region property, polymer flooding, enhanced oil recovery

AMS subject classifications. 65M12, 65M60, 76S05

DOI. 10.1137/17M1125820

1. Introduction.

1.1. Scope. We are interested in the numerical simulation of two-phase, multicomponent flows in heterogeneous porous media governed by balance laws derived from multiphase mixture theory. From the diverse applications described by such a general framework (including, for instance, tissue growth or paper manufacturing), here we focus on the process of polymer flooding, which is a common mechanism of oil displacement employed in enhanced oil recovery (EOR). In principle, after the so-called secondary oil recovery step (mainly driven by water flooding), a large amount of oil still remains trapped within the rock (see, e.g., [35] and the references therein). Then polymer flooding consists in adding a certain amount of polymers to water to be injected to increase the viscosity of the aqueous phase and, thereby, to improve the mobility of the oil and to increase the volumetric sweep efficiency of the reservoir flooding.

*Submitted to the journal's Computational Methods in Science and Engineering section April 17, 2017; accepted for publication (in revised form) November 28, 2017; published electronically April 24, 2018.

http://www.siam.org/journals/sisc/40-2/M112582.html

Funding: This work was partially supported by BASAL project CMM, Universidad de Chile and Centro de Investigación en Ingeniería Matemática (CI^{2}MA), Universidad de Concepción; by Fondecyt projects 1170473 and 3150313; by CRHIAM, project CONICYT/FONDAP/15130015; by the EPSRC through the research grant EP/R00207X/1; and by the Dirección de Investigación y Desarrollo of Universidad de La Serena through DIDULS project PR17151.

†CI^{2}MA and Departamento de Ingeniería Matemática, Universidad de Concepción, Casilla 160-C, Concepción, Chile (rburger@ing-mat.udec.cl).

‡Department of Mathematics, Indian Institute of Technology Guwahati, Guwahati, 781039, India (sudarshan.k@iitg.ernet.in).

§Mathematical Institute, Oxford University, Andrew Wiles Building, Woodstock Road, OX2 6GG Oxford, UK (ruizbaier@maths.ox.ac.uk).

¶Departamento de Matemáticas, Universidad de La Serena, Av. Cisternas 1200, La Serena, Chile (htorres@userena.cl).

Fluid flow in the reservoir is mainly driven by the heterogeneity of the medium and mobility difference between the involved phases. These mechanisms produce a complex structure arising from the nonlinearities of the flow, intrinsic fluid properties, and interaction with transport processes. Thus, any numerical scheme targeted for such applications needs to be sufficiently accurate to handle the flow process, high nonlinearities, medium heterogeneities, complex reservoir geometry, and high gradients of volume fractions.

Let us consider an open and bounded domain $\Omega \subset \mathbb{R}^2$ with Lipschitz boundary $\partial\Omega$, where the processes of multicomponent flow with adsorption are supposed to occur. There it is assumed that three fluid components, namely, oil, water, and polymers, flow and interact within two phases: aqueous (wetting, "w") and oleic (nonwetting, "n"), of respective saturations s_{w} and s_{n} such that $s_{\mathrm{w}} + s_{\mathrm{n}} = 1$. The oleic phase consists of oil only, whereas the aqueous phase is conformed by both water and the mixture of $\mathcal{M}$ types of injected polymers of concentrations (mass fractions) $c_1, \ldots, c_{\mathcal{M}}$. We further suppose that the fluids are incompressible, immiscible, and there are no sources or sinks, and since our main focus is on reservoir-scale simulation, capillary pressure is neglected in the formulation of the model and the numerical scheme. The phasic conservation of mass now yields the local continuity equation [8]

$$\varphi \frac{\partial s}{\partial t} + \operatorname{div} \boldsymbol{F} = 0, \quad \boldsymbol{F} = \boldsymbol{F}(s, \boldsymbol{c}, \boldsymbol{u}, \boldsymbol{x}), \quad \boldsymbol{c} := (c_1, \ldots, c_{\mathcal{M}})^{\mathrm{T}}, \tag{1.1}$$

where $s := s_{\mathrm{w}}$, t is time, φ is the rock porosity (assumed constant), and the nonlinear flux vector $\boldsymbol{F}$ depends on s, the concentrations of polymers $\boldsymbol{c}$, the volume average flow velocity $\boldsymbol{u}$, and spatial position $\boldsymbol{x}$. Under the same assumptions, the transport of the polymers in the aqueous phase (cf., e.g., [30,38]) is described by the continuity equations

$$\varphi \frac{\partial}{\partial t}(s c_l) + \frac{\partial}{\partial t}\big((1-\varphi)\rho_{\mathrm{r}} a_l(c_l)\big) + \operatorname{div}(c_l \boldsymbol{F}) = 0, \quad l = 1, \ldots, \mathcal{M}, \tag{1.2}$$

where ρ_{r} is the density of rock and $a_l(c_l)$ is the adsorption of polymer c_l per unit mass of the rock. The precise algebraic definition of $\boldsymbol{F}$ and $a_1, \ldots, a_{\mathcal{M}}$ is provided in section 2.1. Note that the transport equations (1.1) and (1.2) are nonlinearly coupled in $s = s(\boldsymbol{x}, t)$ and $\boldsymbol{c} = \boldsymbol{c}(\boldsymbol{x}, t)$. In addition, the flux function $\boldsymbol{F}$ usually depends discontinuously on $\boldsymbol{x}$ since the porous medium is heterogeneous. Finally, the volume average flow velocity $\boldsymbol{u}$ is determined from the following Brinkman model [6] that represents the momentum and mass conservation of the mixture:

$$\begin{aligned} \boldsymbol{K}(\boldsymbol{x})^{-1}\boldsymbol{u} - \mathbf{div}\big(\mu(s,\boldsymbol{c})\boldsymbol{\varepsilon}(\boldsymbol{u}) - p\boldsymbol{I}\big) &= (\rho_{\mathrm{w}} - \rho_{\mathrm{n}}) s \boldsymbol{g}, \\ \operatorname{div} \boldsymbol{u} &= j, \end{aligned} \tag{1.3}$$

where p is the pressure field, $\boldsymbol{g} = (0, -g)^{\mathrm{T}}$ is the gravitational acceleration, and j is a mass source or sink in the system. Here $\boldsymbol{K}(\boldsymbol{x})$ is the absolute permeability tensor of the medium, $\mu(s,\boldsymbol{c})\varepsilon(\boldsymbol{u}) - p\boldsymbol{I}$ is the Cauchy stress tensor, $\boldsymbol{\varepsilon}(\boldsymbol{u}) = \frac{1}{2}(\nabla \boldsymbol{u} + \nabla \boldsymbol{u}^{\mathrm{T}})$ is the infinitesimal rate of strain and $\mu = \mu(s,\boldsymbol{c})$ is the viscosity (inverse of the total mobility, defined below) that is assumed uniformly bounded here. The constants ρ_{w} and ρ_{n} are the densities of the aqueous and oleic phases, respectively. In the case of an isotropic medium, the permeability tensor reduces to $\boldsymbol{K} = \kappa(\boldsymbol{x})\boldsymbol{I}$, where κ is a scalar function (assumed uniformly bounded $0 < \kappa_{\min} \leq \kappa(\boldsymbol{x}) \leq \kappa_{\max} < \infty$), and $\boldsymbol{I}$ is the 2×2 identity matrix. Thus, the problem at hand consists in determining the $\mathcal{M} + 4$ scalar components of s, $\boldsymbol{c}$, $\boldsymbol{u}$, and p as functions of $\boldsymbol{x}$ and t from the coupled

system (1.1)–(1.3) of the same numbers of scalar PDEs, supplied with suitable initial and boundary conditions.

Although we neglect capillary pressure and dispersion terms, the predominance of different processes might change the mathematical character of (1.1)–(1.3). In addition, the transport of the polymers is coupled to the phase equations, it changes the phase viscosity, and hence alters flow patterns in the system. To solve (1.1)–(1.3) along with suitable initial and boundary conditions, we here adopt a discontinuous Galerkin (DG) discretization: a DG approximation is introduced for the transport equations (1.1), (1.2) and we utilize an $\mathbf{H}(\mathrm{div})$-conforming DG method for the flow equations (1.3) based on the treatment of the Brinkman equations by Könnö and Stenberg [23]. DG methods feature desirable properties for the present application: flexibility for *hp*-refinement, locking-free approximations, ability to handle discontinuous coefficients, sharp solution interface capturing, and many others (see [40] for their application to a similar transport-flow problem). Moreover, the phenomenon at hand suggests that fluxes may be discontinuous, and such a feature will be imposed also on the numerical fluxes across element boundaries, following the approach of [39] that is here adapted to unstructured simplicial meshes. A Newton method is employed to resolve the main nonlinearity in the transport equations (more precisely, in the isothermal adsorption term). The time discretization of the transport problem utilizes a third-order strong stability preserving Runge–Kutta (SSP-RK) method, and the coupling with the flow equations is handled by a sequential iteration scheme. This choice is mainly driven by computational cost and memory requirements (that are usually much higher in the fully coupled approach).

1.2. Related work. The main novel contributions in this paper consist in combining high-order space discretizations (which are, moreover, well suited for parallelization and useful in large scale EOR simulations) with RK methods, specially targeted for a large class of multicomponent flow problems; and in the analysis of the proposed methods in terms of invariance properties of the discrete saturation and concentration fields. From the modeling point of view, we combine the transport-adsorption submodel, usually considered as a spatially one-dimensional system of conservation laws, with the multidimensional Brinkman model of viscous flow in porous media.

To put these advances into the proper perspective, we recall that the flow of the fluid components is described by an extension of the two-phase Buckley–Leverett model [8] arising from a fractional flow analysis [30]. Such a model was analyzed as a hyperbolic system of conservation laws in [19], first without adsorption. The Riemann problem of the multicomponent model with adsorption was solved in [20, 21]. The additional difficulties due to the nonlinear adsorption terms within the time derivative are treated in [34, sect. 1.8] and [39], while those caused by the nonstrict hyperbolicity of the underlying system of conservation laws are addressed in [22]. All the works cited so far handle the transport-adsorption submodel (1.1), (1.2) in one space dimension, which avoids the necessity of computing the flow field of the mixture.

Here, that system of mass conservation equations is coupled to a mass and momentum equation for the mixture. In the regime we are interested in, it suffices to incorporate the Stokes–Darcy (or Brinkman) approximation of viscous flow in porous media. Discretizations involving discontinuous elements in combination with finite volume element methods and applied to flow-transport equations in similar contexts include a "black oil" (oil-water-gas) model without adsorption [4], finite volume element methods for applications to sedimentation processes where the flow is governed

by the Stokes equations [10, 11], finite-volume-based linearization schemes for two-phase flow described by Darcy's law [31, 32], error estimates for degenerate parabolic equations arising in a model of reactive solute transport in porous media [3], convergence of mixed finite element schemes for porous media solute transport model [32], a version of the sedimentation-consolidation model treated in [11] that is described by the Navier–Stokes equations [37], a treatment of a related variable density problem where the flow is also governed by the Navier–Stokes equations [12], the approximation of a two-dimensional parabolic integro-differential equation as a model problem for flow in porous media [16], incompressible miscible displacement in porous media governed by explicit pressure-velocity relationships [25, 27], and a general class of multicontinuum models derived from mixture theory [36].

We mention that our approach, and that of most of the cited works, does not distinguish between different length scales that on one end would allow for an accurate description of pore-level petrophysical properties and on the other end permit effective simulation of the global dynamics at reservoir scale. A multiscale simulator for polymer flooding that handles these issues is advanced in [18]. If capillary pressure is present, then another possibility for simulation of two-phase flow and transport in porous media are iterative implicit pressure-explicit saturation techniques [24] that involve the solution of nonlinear algebraic equations at each time step. A robust linearization method to handle these issues, called L-scheme, was recently proposed [33].

1.3. Outline of the paper. The remainder of the paper is organized as follows. Section 2 contains an overview of the model problem and the governing equations we will advocate to. The mixed $\mathbf{H}(\mathrm{div})$-conforming DG method for the flow equations, for a fixed pair of saturation and concentrations, is stated in section 3. Next, the DG scheme for the transport equations is presented in section 4. We derive the semidiscrete and fully discrete methods, and make precise the choice of discontinuous numerical fluxes. In section 5 we establish an invariant region property of the transport DG discretization, and in section 6 we collect a series of numerical tests illustrating convergence, stability, and performance of the proposed scheme in simplified and more application-oriented cases.

2. Preliminaries.

2.1. Flux vector and adsorption functions. Polymer adsorption determines the success of polymer flooding both technically and economically [14]. This process is modeled here through the terms $a_1, \ldots, a_{\mathcal{M}}$ that could be functions of salinity, polymer concentration, and permeability. For simplicity, in most numerical experiments we adopt the simple Langmuir-type isotherms

$$a_l(c_l) = c_l^{\max} \frac{b c_l}{1 + b c_l}, \quad l = 1, \ldots, \mathcal{M},$$

(see [29]), where b is a Langmuir constant and $c_l^{\max}$ is the maximum concentration of polymer component l adsorbed to the rock, which will be specified later. An alternative expression is the Freundlich isotherm, which we may here state as

$$a_l(c_l) = c_l^{\max} c_l^{\alpha_{\mathrm{F}}}, \quad \alpha_{\mathrm{F}} \in (0, 1], \quad l = 1, \ldots, \mathcal{M}. \tag{2.1}$$

The properties and support for each of these and other isotherms are widely discussed in [29, sect. 4.5].

The nonlinear flux vector $\boldsymbol{F} = \boldsymbol{F}(s, \boldsymbol{c}, \boldsymbol{u}, \boldsymbol{x})$ takes the form

$$\boldsymbol{F}(s, \boldsymbol{c}, \boldsymbol{u}, \boldsymbol{x}) = f(s, \boldsymbol{c})\boldsymbol{u} + b(s, \boldsymbol{c})\boldsymbol{K}(\boldsymbol{x})\boldsymbol{g},$$

where f is the fractional flow function related to the aqueous phase given by

$$f(s,\boldsymbol{c}) := \frac{\lambda_{\rm w}(s,\boldsymbol{c})}{\lambda_{\rm w}(s,\boldsymbol{c})+\lambda_{\rm n}(s)},$$

and $b(s,\boldsymbol{c}) := f(s,\boldsymbol{c})\lambda_{\rm n}(s)(\rho_{\rm w}-\rho_{\rm n})$. The corresponding phase mobilities $\lambda_{\rm w}$ and $\lambda_{\rm n}$ are expressed in terms of the phase relative permeabilities $k_{\rm rw}$ and $k_{\rm rn}$ and the phase viscosities $\mu_{\rm w}$ and $\mu_{\rm n}$, namely, $\lambda_{\rm w} = k_{\rm rw}/\mu_{\rm w}$ and $\lambda_{\rm n} = k_{\rm rn}/\mu_{\rm n}$, and we define $\lambda_{\rm total} := \lambda_{\rm w}+\lambda_{\rm n}$ and $\mu(s,\boldsymbol{c}) := 1/\lambda_{\rm total}$. For the relative permeabilities we use the Brooks–Corey model [7], as implemented in [38]. The viscosity $\mu_{\rm n}$ is kept constant as the flow is immiscible and polymers are transported only through the aqueous phase. The viscosity $\mu_{\rm w} = \mu_{\rm w}(\boldsymbol{c})$ of the wetting phase depends on the concentration of the polymers and we adopt an expression for $\mu_{\rm w}$ as presented in [38, p. 433], namely,

$$\mu_{\rm w}(\boldsymbol{c}) = \mu_{\rm w,0} + aC, \tag{2.2}$$

where $\mu_{\rm w,0}$ is the viscosity of the wetting phase in the absence of polymers and C is a scalar variable that can be chosen as $C = c_1 + \cdots + c_{\mathcal{M}}$ and a is a positive constant. The original treatment [38], and some of our examples, however, are limited to $\mathcal{M} = 1$.

2.2. Initial and boundary conditions. Adequate initial and boundary data complementing (1.1)–(1.3) are necessary to close the system. We will consider a constant initial saturation and concentrations s_0, $c_{l,0}$, a boundary saturation and concentration are assumed on a part of the boundary identified as the inlet, and on the remainder of the boundary we impose zero-flux conditions for the saturation and concentrations, together with either Dirichlet conditions for the velocity, or Dirichlet conditions for the pressure field. The presentation of the discretization will focus on the case of homogeneous Dirichlet velocity and zero-flux saturation and concentration.

3. Mixed H(div)-conforming DG discretization for the Brinkman problem. Let us consider a fixed pair of saturation-concentration functions $s, \boldsymbol{c}$ such that $\mu(s,\boldsymbol{c})$ is positive and bounded, i.e.,

$$\mu_{\min} \le \mu(s,\boldsymbol{c}) \le \mu_{\max}$$

with constants $0 < \mu_{\min}, \mu_{\max} < \infty$. We denote standard spaces by $\mathbf{H} := \mathbf{H}^1_0(\Omega) = \{\boldsymbol{v} \in \mathbf{H}^1(\Omega) : \boldsymbol{v} = \mathbf{0} \text{ on } \partial\Omega\}$, $Q := L^2_0(\Omega) = \{q \in L^2(\Omega) : (q,1)_\Omega = 0\}$, multiply (1.3) by suitable test functions $(\boldsymbol{v}, q) \in \mathbf{H} \times Q$, and integrate the result by parts in such a way that the weak form of (1.3) is as follows: find $(\boldsymbol{u}, p) \in \mathbf{H} \times Q$ such that

$$\mathcal{S}^{s,\boldsymbol{c}}\big((\boldsymbol{u},p),(\boldsymbol{v},q)\big) = \mathcal{F}^s(\boldsymbol{v},q) \qquad \forall (\boldsymbol{v},q) \in \mathbf{H}\times Q, \tag{3.1}$$

where the involved forms and functionals are defined for all $(\boldsymbol{u},p),(\boldsymbol{v},q) \in \mathbf{H}\times Q$ as

$$\begin{gathered}
\mathcal{S}^{s,\boldsymbol{c}}\big((\boldsymbol{u},p),(\boldsymbol{v},q)\big) := a^{s,\boldsymbol{c}}(\boldsymbol{u},\boldsymbol{v}) + b(\boldsymbol{v},p) + b(\boldsymbol{u},q),\\
\mathcal{F}^s(\boldsymbol{v},q) := \big((\rho_{\rm w}-\rho_{\rm n})s\boldsymbol{g},\boldsymbol{v}\big)_\Omega - (j,q)_\Omega,\\
a^{s,\boldsymbol{c}}(\boldsymbol{u},\boldsymbol{v}) := (\boldsymbol{K}^{-1}\boldsymbol{u},\boldsymbol{v})_\Omega + \big(\mu(s,\boldsymbol{c})\boldsymbol{\varepsilon}(\boldsymbol{u}),\boldsymbol{\varepsilon}(\boldsymbol{v})\big)_\Omega, \quad b(\boldsymbol{v},q) := -(\operatorname{div}\boldsymbol{v},q)_\Omega.
\end{gathered}$$

The discretization of (1.3) will seek discrete velocities in an $\mathbf{H}(\operatorname{div},\Omega)$-conforming finite-dimensional space $\mathbf{H}_h$, associated with a regular partition $\mathcal{T}_h$ of Ω into triangles. We recall that a family of triangulations $\mathcal{F} = \{\mathcal{T}_h\}_{h>0}$ is regular if

$$\exists \sigma > 0 : \quad m_K \ge \sigma h_K \quad \forall K \in \mathcal{T}_h \quad \forall \mathcal{T}_h \in \mathcal{F}, \tag{3.2}$$

where h_K is the diameter of a generic element $K \in \mathcal{T}_h$ and m_K is that of the largest circle inscribed in K. For all $K \in \mathcal{T}_h$ and $e \subset \partial K$, we denote by $\boldsymbol{n}_e$ the normal vector to e outward to K. The set of neighbors of $K \in \mathcal{T}_h$ will be denoted by $\mathcal{N}_K$. If $L \in \mathcal{N}_K$ is the element sharing with K the edge $e = K|L$, then the normal is denoted componentwise as $\boldsymbol{n}_e = \boldsymbol{n}_{K|L} = (n^1_{K|L}, n^2_{K|L})^{\mathrm{T}}$. We denote by $\mathcal{E}_h$ the set of all edges of all $K \in \mathcal{T}_h$.

We here choose Brezzi–Douglas–Marini elements of degree one [5] to approximate $\boldsymbol{u}$, and piecewise constant approximations of p, that is,

$$\begin{aligned}
\mathbf{H}_h &= \big\{\boldsymbol{v} \in \mathbf{H}(\mathrm{div}, \Omega) : \boldsymbol{v}|_K \in \mathbb{P}_1(K)^2 \ \forall K \in \mathcal{T}_h \text{ and } \boldsymbol{v} \cdot \boldsymbol{n} = 0 \text{ on } \partial\Omega\big\},\\
Q_h &= \big\{q \in L^2_0(\Omega) : q|_K \in \mathbb{P}_0(K) \ \forall K \in \mathcal{T}_h\big\},
\end{aligned}$$

which satisfy $\mathrm{div}\, \mathbf{H}_h \subset Q_h$ (see [23]). As usual, $\mathbb{P}_k(K)$ denotes the space spanned by polynomials of degree less than or equal to k. Since $\mathbf{H}_h$ is not a subspace of $\mathbf{H}$, additional terms are required in the discrete formulation in order to ensure stability. We adapt to our configuration the interior penalty method introduced in [23], consisting in replacing the bilinear form $a^{s,\boldsymbol{c}}(\cdot,\cdot)$ by its mesh-dependent counterpart

$$\begin{aligned}
a_h^{s,\boldsymbol{c}}(\boldsymbol{u}_h, \boldsymbol{v}_h) := (\boldsymbol{K}^{-1}\boldsymbol{u}_h, \boldsymbol{v}_h)_\Omega + \sum_{K\in\mathcal{T}_h} \big(\mu(s,\boldsymbol{c})\boldsymbol{\varepsilon}(\boldsymbol{u}_h), \boldsymbol{\varepsilon}(\boldsymbol{v}_h)\big)_K\\
+ \sum_{e\in\mathcal{E}_h}\left(\frac{\alpha}{h_e}\big\langle[\![\mu(s,\boldsymbol{c})\boldsymbol{u}_h]\!], [\![\boldsymbol{v}_h]\!]\big\rangle_e - \big\langle\{\!\{\mu(s,\boldsymbol{c})\boldsymbol{\varepsilon}(\boldsymbol{u}_h)\boldsymbol{n}\}\!\}, [\![\boldsymbol{v}_h]\!]\big\rangle_e\right.\\
\left. - \big\langle\{\!\{\mu(s,\boldsymbol{c})\boldsymbol{\varepsilon}(\boldsymbol{v}_h)\boldsymbol{n}\}\!\}, [\![\boldsymbol{u}_h]\!]\big\rangle_e\right)
\end{aligned}$$

for a given stabilization parameter $\alpha > 0$, where the standard symbols $[\![\cdot]\!]$ and $\{\!\{\cdot\}\!\}$ denote the jump and mean values, respectively, of a vectorial quantity across a point on e. The $\mathbf{H}(\mathrm{div})$-conforming DG method associated with (3.1) can now be formulated as follows: for fixed saturation and polymer concentration functions s and $\boldsymbol{c}$, find $(\boldsymbol{u}_h, p_h) \in \mathbf{H}_h \times Q_h$ such that

$$\mathcal{S}_h^{s,\boldsymbol{c}}\big((\boldsymbol{u}_h, p_h), (\boldsymbol{v}_h, q_h)\big) = \mathcal{F}^s(\boldsymbol{v}_h, q_h) \qquad \forall (\boldsymbol{v}_h, q_h) \in \mathbf{H}_h \times Q_h, \tag{3.3}$$

where we define

$$\mathcal{S}_h^{s,\boldsymbol{c}}\big((\boldsymbol{u}_h, p_h), (\boldsymbol{v}_h, q_h)\big) := a_h^{s,\boldsymbol{c}}(\boldsymbol{u}_h, \boldsymbol{v}_h) + b(\boldsymbol{v}_h, p_h) + b(\boldsymbol{u}_h, q_h).$$

The solvability, consistency, and stability of this formulation, along with a priori and a posteriori error bounds for (3.3), have been derived in [23]. The suggested energy norms depend on the mesh size h and, as in [23], also on the permeability and viscosity:

$$\begin{aligned}
\|\boldsymbol{v}\|_h^2 &:= \|\boldsymbol{v}\|_{0,\Omega}^2 + \eta\left(\sum_{K\in\mathcal{T}_h}\|\boldsymbol{\varepsilon}(\boldsymbol{v})\|_{0,K}^2 + \sum_{e\in\mathcal{E}_h}\frac{1}{h_e}\|[\![\boldsymbol{v}\cdot\boldsymbol{t}]\!]\|_{0,e}^2\right),\\
\|q\|_h^2 &:= \|q\|_{0,\Omega}^2 + \sum_{e\in\mathcal{E}_h}\frac{h_e}{h_e^2+\eta}\|[\![q]\!]\|_{0,e}^2,
\end{aligned} \tag{3.4}$$

where $\eta = \kappa_{\max}\mu_{\max}$, h_e is the length of a given edge $e \in \mathcal{E}_h$, and $\boldsymbol{t}$ denotes the tangent vector on e.

4. A DG method for the transport equations.

4.1. General formulation and semidiscrete approximation. We multiply the transport equations (1.1) and (1.2) by $\phi_s, \phi_{c_l} \in V := H^1(\Omega)$, respectively, where $l = 1, \dots, \mathcal{M}$, and integrate the results by parts over an arbitrary subset $R \subset \Omega$ to obtain the following local weak formulation, where $\boldsymbol{F}(s, \boldsymbol{c}, \boldsymbol{u}) := \boldsymbol{F}(s, \boldsymbol{c}, \boldsymbol{u}, \cdot)$:

$$
\begin{aligned}
&\frac{\mathrm{d}}{\mathrm{d}t}(\varphi s, \phi_s)_R - \big(\boldsymbol{F}(s, \boldsymbol{c}, \boldsymbol{u}), \nabla\phi_s\big)_R + \big\langle \boldsymbol{F}(s, \boldsymbol{c}, \boldsymbol{u}) \cdot \boldsymbol{n}_R, \phi_s \big\rangle_{\partial R} = 0, \\
&\frac{\mathrm{d}}{\mathrm{d}t}\big(\varphi s c_l + (1-\varphi)\rho_{\mathrm{r}} a_l(c_l), \phi_{c_l}\big)_R - \big(c_l \boldsymbol{F}(s, \boldsymbol{c}, \boldsymbol{u}), \nabla\phi_{c_l}\big)_R \\
&\qquad + \big\langle c_l \boldsymbol{F}(s, \boldsymbol{c}, \boldsymbol{u}) \cdot \boldsymbol{n}_R, \phi_{c_l} \big\rangle_{\partial R} = 0, \quad l = 1, \dots, \mathcal{M},
\end{aligned}
\tag{4.1}
$$

and where $\boldsymbol{n}_R$ denotes the outward unit normal to ∂R. Next, we introduce the following finite element space (nonconforming to V) for $k > 0$:

$$
V_h := \big\{ \phi \in L^2(\Omega) : \phi|_K \in \mathbb{P}_k(K) \; \forall K \in \mathcal{T}_h \big\},
$$

and denote by $V_h(K)$ its localization to the element K, so that a semidiscrete DG method for (4.1) reads for $0 < t \le T$, and for a fixed discrete velocity $\boldsymbol{u}_h$, find $(s_h(t), \boldsymbol{c}_h(t)) \in V_h \times V_h^{\mathcal{M}}$ such that for a given $K \in \mathcal{T}_h$,

$$
\begin{aligned}
&\frac{\mathrm{d}}{\mathrm{d}t}(\varphi s_h, \phi_s)_K - \big(\boldsymbol{F}(s_h, \boldsymbol{c}_h, \boldsymbol{u}_h), \nabla\phi_s\big)_K \\
&\qquad + \big\langle \boldsymbol{F}(s_h, \boldsymbol{c}_h, \boldsymbol{u}_h) \cdot \boldsymbol{n}_K, \phi_s \big\rangle_{\partial K} = 0 \quad \forall \phi_s \in V_h(K),
\end{aligned}
\tag{4.2}
$$

$$
\begin{aligned}
&\frac{\mathrm{d}}{\mathrm{d}t}\big(\varphi s_h c_{lh} + (1-\varphi)\rho_{\mathrm{r}} a_l(c_{lh}), \phi_{c_l}\big)_K - \big(c_{lh} \boldsymbol{F}(s_h, \boldsymbol{c}_h, \boldsymbol{u}_h), \nabla\phi_{c_l}\big)_K \\
&\qquad + \big\langle c_{lh} \boldsymbol{F}(s_h, \boldsymbol{c}_h, \boldsymbol{u}_h) \cdot \boldsymbol{n}_K, \phi_{c_l} \big\rangle_{\partial K} = 0 \quad \forall \phi_{c_l} \in V_h(K), \quad l = 1, \dots, \mathcal{M},
\end{aligned}
\tag{4.3}
$$

where the expressions $\boldsymbol{F}(s_h, \boldsymbol{c}_h, \boldsymbol{u}_h) \cdot \boldsymbol{n}_K$ and $c_{lh}\boldsymbol{F}(s_h, \boldsymbol{c}_h, \boldsymbol{u}_h) \cdot \boldsymbol{n}_K$, $l = 1, \dots, \mathcal{M}$, will be approximated by numerical fluxes $\hat{F}$ and $\hat{G}_1, \dots, \hat{G}_{\mathcal{M}}$, respectively, that are specified in the next section.

4.2. Choice of numerical fluxes. In this section (and whenever clear from the context) the explicit dependence on the time variable will be dropped. As in [13], we approximate the component of the exact flux normal to an edge $e \subset \partial K$ of element K with outer normal $\boldsymbol{n}_e$ as

$$
\boldsymbol{F}(s_h, \boldsymbol{c}_h, \boldsymbol{u}_h) \cdot \boldsymbol{n}_e \approx \hat{F}\big(s_h(\check{\boldsymbol{x}}^K), s_h(\hat{\boldsymbol{x}}^K), \boldsymbol{c}_h(\check{\boldsymbol{x}}^K), \boldsymbol{c}_h(\hat{\boldsymbol{x}}^K), \boldsymbol{u}_h, \boldsymbol{n}_e\big),
$$

where $\phi_h(\check{\boldsymbol{x}}^K)$ and $\phi_h(\hat{\boldsymbol{x}}^K)$ represent the traces of the approximate generic field ϕ (e.g., concentration and saturation) taken from the interior and exterior of K, respectively. Note that it suffices to specify $\hat{F}$ to make precise the flux definitions in (4.2), and here we employ discontinuous fluxes as proposed in [39], together with the numerical flux formulation of [9, section 3.4]. There, one treats $\boldsymbol{c}_h$ as an elementwise constant datum, so on each $e \subset \partial K$ we employ

$$
\hat{F}\big(\alpha, \beta, \boldsymbol{c}_h(\check{\boldsymbol{x}}^K), \boldsymbol{c}_h(\hat{\boldsymbol{x}}^K), \boldsymbol{u}_h, \boldsymbol{n}_e\big) = \hat{F}_1(\alpha, \beta, n_e^1) + \hat{F}_2(\alpha, \beta, n_e^2),
\tag{4.4}
$$

where the contributions $\hat{F}_1$ and $\hat{F}_2$ are the DFLU numerical fluxes [1] computed as follows. According to the assumption of two space dimensions, we have $\boldsymbol{F} = (F_1, F_2)^{\mathrm{T}}$,

and for $\boldsymbol{n}_e = (n_e^1, n_e^2)^{\mathrm{T}}$ and any saturation value s, we define

$$\begin{aligned}\boldsymbol{F}\big(s, \boldsymbol{c}_h(\check{\boldsymbol{x}}^K), \boldsymbol{u}_h\big)\cdot\boldsymbol{n}_e &= F_1\big(s, \boldsymbol{c}_h(\check{\boldsymbol{x}}^K), \boldsymbol{u}_h\big)n_e^1 + F_2\big(s, \boldsymbol{c}_h(\check{\boldsymbol{x}}^K), \boldsymbol{u}_h\big)n_e^2\\ &=: F_{e,1}^-(s) + F_{e,2}^-(s),\\ \boldsymbol{F}\big(s, \boldsymbol{c}_h(\hat{\boldsymbol{x}}^K), \boldsymbol{u}_h\big)\cdot\boldsymbol{n}_e &= F_1\big(s, \boldsymbol{c}_h(\hat{\boldsymbol{x}}^K), \boldsymbol{u}_h\big)n_e^1 + F_2\big(s, \boldsymbol{c}_h(\hat{\boldsymbol{x}}^K), \boldsymbol{u}_h\big)n_e^2\\ &=: F_{e,1}^+(s) + F_{e,2}^+(s).\end{aligned}$$

Since the quantities $F_{e,i}^{\pm}$ satisfy the hypotheses (H_1) and (H_2) of [1], the DFLU numerical fluxes are in the present case given by

$$\hat{F}_i(\alpha,\beta,n^i) = \gamma^i \max\big\{\gamma^i F_i^-(\gamma^i\delta_i^1), \gamma^i F_i^+(\gamma^i\delta_i^2)\big\}, \quad \gamma^i := \operatorname{sgn}(n^i), \quad i = 1,2, \tag{4.5}$$

where we have replaced n_e^i and $F_{e,i}^{\pm}$ by n^i and $F_i^{\pm}$, respectively, and set, for $i = 1, 2$,

$$\delta_i^1 := \max\big\{\gamma^i\alpha, \gamma^i\theta_{F_i^-}\big\}, \quad \delta_i^2 := \min\big\{\gamma^i\beta, \gamma^i\theta_{F_i^+}\big\},$$

where $\theta_{F_i^{\pm}}$ are chosen such that

$$F_i^{\pm}(\theta_{F_i^{\pm}}) = \min_{0\le\phi\le 1}\big(\gamma^i F_i^{\pm}(\phi)\big).$$

LEMMA 4.1. *For fixed values of $\boldsymbol{u}_h$, $\boldsymbol{c}_h(\check{\boldsymbol{x}}^K)$, and $\boldsymbol{c}_h(\hat{\boldsymbol{x}}^K)$, the numerical flux $\hat{F}$ defined by* (4.4) *is monotone (i.e., it is a nondecreasing function of α and a nonincreasing function of β) and conservative, that is*

$$\hat{F}\big(\alpha,\beta,\boldsymbol{c}_h(\check{\boldsymbol{x}}^K),\boldsymbol{c}_h(\hat{\boldsymbol{x}}^K),\boldsymbol{u}_h,\boldsymbol{n}\big) = -\hat{F}\big(\beta,\alpha,\boldsymbol{c}_h(\check{\boldsymbol{x}}^K),\boldsymbol{c}_h(\hat{\boldsymbol{x}}^K),\boldsymbol{u}_h,-\boldsymbol{n}\big).$$

The proof of Lemma 4.1 follows along the lines of [9].

In addition, the numerical fluxes

$$c_{lh}\boldsymbol{F}(s_h,\boldsymbol{c}_h,\boldsymbol{u}_h)\cdot\boldsymbol{n}_K \approx \hat{G}_l, \quad l = 1,\dots,\mathcal{M},$$

arising in (4.3) are defined as follows:

$$\hat{G}_l = \begin{cases} c_{lh}(\check{\boldsymbol{x}}^K)\hat{F} & \text{if } \hat{F} > 0,\\ c_{lh}(\hat{\boldsymbol{x}}^K)\hat{F} & \text{otherwise,}\end{cases} \qquad l = 1,\dots,\mathcal{M},$$

depending on the characteristic speed of the local polymer concentrations c_{lh} (see [39, section 2]). We note that the numerical fluxes $\hat{F}$ and $\hat{G}_1,\dots,\hat{G}_{\mathcal{M}}$ are not consistent in the usual sense as the corresponding flux functions are discontinuous in $\boldsymbol{x}$. However, this does not compromise the possibility of deriving convergence of the scheme, because stability still holds (see [2, p. 181]).

4.3. Fully discrete scheme for the transport equations. We insert the corresponding numerical fluxes $\hat{F}$ and $\hat{G}_l$ into the expressions (4.2) and (4.3) and approximate the boundary and interior integrals by suitable quadrature formulas over each edge e of an element K. Specifically, for ease of notation we denote for a given element K and interior node $\boldsymbol{x}_i^K$, $i = 1,\dots,\hat{p}$, the argument of $\boldsymbol{F}$ by

$$\boldsymbol{y}_{K,i,h}(t) := \big(s_h(\boldsymbol{x}_i^K,t), \boldsymbol{c}_h(\boldsymbol{x}_i^K,t), \boldsymbol{u}_h, \boldsymbol{x}_i^K\big),$$

and for each element K, edge $e = K|L \subset \partial K$ and boundary node $\boldsymbol{x}_i^e$, $i = 1, \dots, \hat{q}$, the argument of $\hat{F}$ and $\hat{G}_l$, $l = 1, \dots, \mathcal{M}$, by

$$\boldsymbol{w}_{e,i,h}(t) := \big(s_h(\check{\boldsymbol{x}}_i^e, t), s_h(\hat{\boldsymbol{x}}_i^e, t), \boldsymbol{c}_h(\check{\boldsymbol{x}}_i^e, t), \boldsymbol{c}_h(\hat{\boldsymbol{x}}_i^e, t), \boldsymbol{u}_h^e, \boldsymbol{x}_i^e, \boldsymbol{n}_e\big).$$

Then (4.2) and (4.3) are approximated as follows, where without loss of generality we choose $\phi_h = \phi_s = \phi_{c_l}$:

$$\begin{aligned} &\frac{\mathrm{d}}{\mathrm{d}t}(\varphi s_h, \phi_h)_K - \sum_{i=1}^{\hat{p}} \bar{\omega}_i \boldsymbol{F}\big(\boldsymbol{y}_{K,i,h}(t)\big) \cdot \nabla \phi_h(\boldsymbol{x}_i^K)|K| \\ &\qquad + \sum_{e \subset \partial K} \sum_{i=1}^{\hat{q}} \omega_i \hat{F}\big(\boldsymbol{w}_{e,i,h}(t)\big) \phi_h(\boldsymbol{x}_i^e)|e| = 0, \end{aligned} \tag{4.6}$$

$$\begin{aligned} &\frac{\mathrm{d}}{\mathrm{d}t}\big(\pi_{lh}, \phi_h\big)_K - \sum_{i=1}^{\hat{p}} \bar{\omega}_i c_{lh}(\boldsymbol{x}_i^K, t) \boldsymbol{F}\big(\boldsymbol{y}_{K,i,h}(t)\big) \cdot \nabla \phi_h(\boldsymbol{x}_i^K)|K| \\ &\qquad + \sum_{e \subset \partial K} \sum_{i=1}^{\hat{q}} \omega_i \hat{G}_l\big(\boldsymbol{w}_{e,i,h}(t)\big) \phi_h(\boldsymbol{x}_i^e)|e| = 0, \quad l = 1, \dots, \mathcal{M}, \end{aligned} \tag{4.7}$$

where $\pi_{lh} := \varphi s_h c_{lh} + (1 - \varphi)\rho_{\mathrm{r}} a_l(c_{lh})$ and $\bar{\omega}_i$ and ω_i are the weights corresponding to the interior and boundary quadrature points $\boldsymbol{x}_i^K$ and $\boldsymbol{x}_i^e$, respectively. We choose a basis $\{\psi_1, \dots, \psi_J\}$ for the space $\mathbb{P}_k(K)$ and write the approximate variables as

$$s_h(t) = \sum_{j=1}^{J} s_j^K(t)\psi_j, \quad \pi_{lh}(t) = \sum_{j=1}^{J} {\pi_l}_j^K(t)\psi_j \quad \text{in } K, \quad l = 1, \dots, \mathcal{M}.$$

Choosing $\phi_h = \psi_j$, $j = 1, \dots, J$, we can recast (4.6) and (4.7) as the ODE system

$$\frac{\mathrm{d}}{\mathrm{d}t}\varphi \boldsymbol{s}_h^K(t) = -\boldsymbol{A}^{-1}(\boldsymbol{w} + \boldsymbol{z}), \quad \frac{\mathrm{d}}{\mathrm{d}t}\boldsymbol{\pi}_{lh}^K(t) = -\boldsymbol{A}^{-1}(\hat{\boldsymbol{w}}_l + \hat{\boldsymbol{z}}_l), \quad l = 1, \dots, \mathcal{M}, \tag{4.8}$$

where $\boldsymbol{s}_h^K(t) := (s_1^K(t), \dots, s_J^K(t))^{\mathrm{T}}$ and $\boldsymbol{\pi}_{lh}^K(t) := ({\pi_l}_1^K(t), \dots, {\pi_l}_J^K(t))^{\mathrm{T}}$. The entries of the matrix $\boldsymbol{A} = (a_{jk})_{J \times J}$ and the vectors $\boldsymbol{w}$, $\boldsymbol{z}$, $\hat{\boldsymbol{z}}_l$, and $\hat{\boldsymbol{w}}_l$ are given by

$$a_{jk} = (\psi_j, \psi_k)_K, \quad w_k = -\sum_{i=1}^{\hat{p}} \bar{\omega}_i \boldsymbol{F}\big(\boldsymbol{y}_{K,i,h}(t)\big) \cdot \nabla \psi_k(\boldsymbol{x}_i^K)|K|,$$

$$z_k = \sum_{e \subset \partial K} \sum_{i=1}^{\hat{q}} \omega_i \hat{F}\big(\boldsymbol{w}_{e,i,h}(t)\big)\psi_k(\boldsymbol{x}_i^e)|e|, \quad \hat{z}_{l,k} = \sum_{e \subset \partial K} \sum_{i=1}^{\hat{q}} \omega_i \hat{G}_l\big(\boldsymbol{w}_{e,i,h}(t)\big)\psi_k(\boldsymbol{x}_i^e)|e|,$$

$$\hat{w}_{l,k} = -\sum_{i=1}^{\hat{p}} \bar{\omega}_i c_{lh}(\boldsymbol{x}_i^K, t) \boldsymbol{F}\big(\boldsymbol{y}_{K,i,h}(t)\big) \cdot \nabla \psi_k(\boldsymbol{x}_i^K)|K|.$$

The semidiscrete system (4.8) is evolved in time with a third-order SSP-RK method [28]. The key point in here is not to split the numerical flux during the SSP-RK stages. Usually the required fluxes are obtained by solution of local Riemann problems for (1.1) and (1.2), or by approximation via a Lax–Friedrichs method. However, the former strategy can be quite expensive in most cases and the latter might be highly inefficient in capturing shocks. Then, following [39] we can derive discontinuous

numerical fluxes for the coupled equations (4.8) by decoupling the system into scalar equations. This is achieved by treating each approximate polymer concentration as a discontinuous coefficient entering the numerical flux (cf. [39, section 2.4]).

The procedure is illustrated for a forward Euler scheme for the coupled equations (4.8), which in turn amounts to determining the value of $\hat{F}$ in the vectors $\boldsymbol{z}_k$ and $\hat{\boldsymbol{z}}_k$ from (4.4), where the arguments are the known saturation, concentrations, and velocity at time t^n. Thereby the values $\boldsymbol{s}_h^K(t^{n+1})$ and $\boldsymbol{\pi}_{l\,h}^K(t^{n+1})$ are computed separately, and the approximate solutions at time t^{n+1} are updated by

$$\begin{aligned} s_h(t^{n+1}) &= (\psi_1,\dots,\psi_L)\boldsymbol{s}_h^K(t^{n+1}) \quad \text{in } K,\\ \pi_{l\,h}(t^{n+1}) &= (\psi_1,\dots,\psi_L)\boldsymbol{\pi}_{l\,h}^K(t^{n+1}) \quad \text{in } K, \quad l=1,\dots,\mathcal{M}. \end{aligned}$$

Then the approximate concentrations $c_{l\,h}(t^{n+1})$ for $l=1,\dots,\mathcal{M}$ are recovered by a Newton method solving

$$\pi_{l\,h}(t^{n+1}) = \varphi s_h(t^{n+1})c_{l\,h}(t^{n+1}) + (1-\varphi)\rho_{\mathrm{r}}a_l\big((c_{l\,h}(t^{n+1})\big), \quad l=1,\dots,\mathcal{M}.$$

5. Invariant region for the discrete transport equations. In this section we assess the L^∞ stability of the DG discretization applied to the coupled system (1.1), (1.2). We will show that the element averages of the DG solutions

$$\bar{s}_K^n := \frac{1}{|K|}\int_K s_h(\boldsymbol{x},t^n)\,\mathrm{d}\boldsymbol{x}, \quad \bar{c}_{l\,K}^{\,n} := \frac{1}{|K|}\int_K c_{l\,h}(\boldsymbol{x},t^n)\,\mathrm{d}\boldsymbol{x}, \quad l=1,\dots,\mathcal{M},$$

satisfy a maximum principle. We recall that in each K the approximate solutions $s_h(t^n)$ and $c_{l\,h}(t^n)$ are polynomials, here denoted by $p_{s,K}^n$ and $p_{c_l,K}^n$, respectively. As the SSP-RK scheme preserves the stability of the forward Euler method for the same time step restriction (see [17, 28]), it suffices to analyze the latter case.

5.1. Invariant region for the discrete saturation. Taking $\phi_h \equiv 1$ and discretizing (4.6) in time with a forward Euler scheme lead to

$$\bar{s}_K^{n+1} = \bar{s}_K^n - \frac{\Delta t}{\varphi|K|}\sum_{e\subset\partial K}\sum_{i=1}^{q}\omega_i\hat{F}_{e,i}|e|, \tag{5.1}$$

where we use the convention $\hat{F}_{e,i} := \hat{F}(\boldsymbol{w}_{e,i,h}(t^n))$. Before applying the same procedure to (4.7), we emphasize that the variables c_l are not conserved; instead, the quantities $\pi_l = \varphi s c_l + (1-\varphi)\rho_{\mathrm{r}}a_l(c_l)$ are conserved. Thus, defining the element average of the conserved quantity π_l at $t=t^n$,

$$\begin{aligned} \bar{\pi}_{l\,K}^{\,n} &:= \frac{1}{|K|}\int_K \pi_{l\,h}(\boldsymbol{x},t^n)\,\mathrm{d}\boldsymbol{x}\\ &= \frac{1}{|K|}\int_K \varphi s_h(\boldsymbol{x},t^n)c_{l\,h}(\boldsymbol{x},t^n) + (1-\varphi)\rho_{\mathrm{r}}a_l\big(c_{l\,h}(\boldsymbol{x},t^n)\big)\,\mathrm{d}\boldsymbol{x}, \end{aligned} \tag{5.2}$$

taking $\phi_h \equiv 1$, and discretizing (4.7) in time with a forward Euler scheme leads to

$$\bar{\pi}_{l\,K}^{\,n+1} = \bar{\pi}_{l\,K}^{\,n} - \frac{\Delta t}{|K|}\sum_{e\subset\partial K}\sum_{i=1}^{q}\omega_i\hat{G}_{l,e,i}|e|, \quad l=1,\dots,\mathcal{M}. \tag{5.3}$$

To recover $\bar{c}_{l\,K}^{\,n+1}$ from $\bar{\pi}_{l\,K}^{\,n+1}$, and following the argument of [2, section 4] in one dimension, we utilize the following lemma.

LEMMA 5.1. *The quantities $\bar{s}_K^n$, $\bar{c}_{l\,K}^n$, and $\bar{\pi}_{l\,K}^n$ are related by*

$$\bar{\pi}_{l\,K}^n = \varphi \bar{s}_K^n \bar{c}_{l\,K}^n + (1-\varphi)\rho_{\mathrm{r}} a_l\big(\bar{c}_{l\,K}^n\big) + \mathcal{O}(h_K). \tag{5.4}$$

Proof. We fix an element $K \in \mathcal{T}_h$ and $l \in \{1, \dots, \mathcal{M}\}$. Using the mean value theorem we can write

$$\int_K s_h(\boldsymbol{x}, t^n) c_{l\,h}(\boldsymbol{x}, t^n)\,\mathrm{d}\boldsymbol{x} = c_{l\,h}(\boldsymbol{x}_0, t^n) \int_K s_h(\boldsymbol{x}, t^n)\,\mathrm{d}\boldsymbol{x} \quad \text{for some } \boldsymbol{x}_0 \in K. \tag{5.5}$$

By a suitable Taylor expansion, we get $c_{l\,h}(\boldsymbol{x}_0, t^n) = \bar{c}_{l\,K}^n + \mathcal{O}(h_K)$. Inserting this into (5.5) and multiplying the result by $1/|K|$ we get

$$\frac{1}{|K|}\int_K s_h(\boldsymbol{x}, t^n) c_{l\,h}(\boldsymbol{x}, t^n)\,\mathrm{d}\boldsymbol{x} = \bar{c}_{l\,K}^n \bar{s}_K^n + \mathcal{O}(h_K). \tag{5.6}$$

Another suitable Taylor expansion yields that

$$\frac{1}{|K|}\int_K a_l\big(c_{l\,h}(\boldsymbol{x}, t^n)\big)\,\mathrm{d}\boldsymbol{x} = a_l\big(\bar{c}_{l\,K}^n\big) + \mathcal{O}(h_K). \tag{5.7}$$

Inserting (5.6) and (5.7) into (5.2) we arrive at (5.4). ∎

Neglecting the $\mathcal{O}(h_K)$ term in (5.4) and utilizing (5.3), we arrive at the following scheme for the concentrations:

$$\begin{aligned} &\bar{s}_K^{n+1}\bar{c}_{l\,K}^{n+1} + \frac{1-\varphi}{\varphi}\rho_{\mathrm{r}} a_l(\bar{c}_{l\,K}^{n+1}) \\ &= \bar{s}_K^n \bar{c}_{l\,K}^n + \frac{1-\varphi}{\varphi}\rho_{\mathrm{r}} a_l(\bar{c}_{l\,K}^n) - \frac{\Delta t}{\varphi|K|}\sum_{e\subset\partial K}\sum_{i=1}^{q}\omega_i \hat{G}_{l,e,i}|e|, \quad l = 1, \dots, \mathcal{M}, \end{aligned}$$

where we have used the convention $\hat{G}_{l,e,i} := \hat{G}_l(\boldsymbol{w}_{e,i,h}(t^n))$, $l = 1, \dots, \mathcal{M}$.

As the edge integrals in (4.6) and (4.7) are to be computed exactly for polynomials of degree $2k+1$ (see [13, Prop. 2.1]), we choose a $(k+1)$-point Gauss rule, where the $q = k+1$ quadrature points corresponding to each edge $e \subset \partial K$ are $\{\boldsymbol{x}_i^e, i = 1, \dots, q\}$.

Next, in order to verify the maximum principle for the discrete saturation resulting from (5.1), one can proceed along the lines of [9]. The key step consists in writing the approximate value as a function of $6q + p$ scalar arguments as follows:

$$\bar{s}_K^{n+1} = H\big(s_h(\check{\boldsymbol{x}}_i^e, t^n), s_h(\hat{\boldsymbol{x}}_i^e, t^n) : i = 1, \dots, q,\ e \subset \partial K;\ s_h(\boldsymbol{x}_j^K, t^n) : j = 1, \dots, p\big). \tag{5.8}$$

The expression (5.8) can be obtained once we formulate the approximate average in terms of the DG solution computed at the quadrature points. Then the concentration can be regarded as a discontinuous coefficient in the numerical flux, so that the following result can readily be proved (following the proof of [9, Lemma 4.1]).

LEMMA 5.2. *The function H in* (5.8) *is increasing in each of its arguments provided the following CFL condition is satisfied, where $\hat{\omega}_1$ is the first weight of the Gauss–Lobatto quadrature rule on $[-1/2, 1/2]$:*

$$\frac{\Delta t}{\varphi|K|}\sum_{e\subset\partial K}|e| \le \frac{2}{3}\hat{\omega}_1. \tag{5.9}$$

If q denotes the number of quadrature points used, then $\hat{\omega}_1 = (1/2-(-1/2))\omega_1/2 = \omega_1/2$, where $\omega_1 = 2/(q(q-1))$ is the quadrature weight corresponding to the interval [-1,1]. For instance, if $q = 3$, then $\hat{\omega}_1 = 1/6$.

In turn, we can assert the following result.

THEOREM 5.1. *The DG solution computed from* (4.2)*, using the DFLU numerical flux* (4.4)–(4.5) *and a forward Euler time stepping, satisfies* $0 \leq \bar{s}_K^{n+1} \leq 1$ *for all* $n \geq 0$*, provided that condition* (5.9) *is met and* $p_{s,K}^n \in [0,1]$*, where* $p_{s,K}^n$ *is the computed DG polynomial at the time step* t^n*.*

We remark that at time t^n, the cellwise DG polynomial $p_{s,K}^n$ need not assume values in $[0,1]$. Therefore, in order to enforce satisfaction of the condition of Theorem 5.1, a *linear* scaling limiter (cf. [9, p. 140]) is applied at the time step t^n. Furthermore, we remark that, a bound on the evolved *complete* DG solution is not guaranteed by Theorem 5.1; the invariant region principle is proved for the *average* only. However, the complete DG solution is used in advancing from each time step. In this respect, the invariant region principle is the least expected result in order to verify the robustness of our method.

5.2. Invariant region for the elementwise concentration. In order to verify whether the computed concentrations lie within the bound of initial concentrations, we first consider a splitting of the numerical fluxes as

$$\begin{aligned}
&\hat{F}_{e,i} = \hat{F}_{e,i}^+ + \hat{F}_{e,i}^-, \quad \text{where } \hat{F}_{e,i}^+ = \max\{0, \hat{F}_{e,i}\} \text{ and } \hat{F}_{e,i}^- = \min\{0, \hat{F}_{e,i}\},\\
&\hat{G}_{e,i} = \check{c}_{e,i}\hat{F}_{e,i}^+ + \hat{c}_{e,i}\hat{F}_{e,i}^-, \quad \text{where } \check{c}_{e,i} = c_h\big(\check{\boldsymbol{x}}_i^e, t\big),\ \hat{c}_{e,i} = c_h\big(\hat{\boldsymbol{x}}_i^e, t\big),
\end{aligned}$$

where, if no confusion arises, we suppress the index l of the concentration and adsorption terms for the rest of this section. In analogy to the analysis for the discrete saturation, here we choose $\phi_h \equiv 1$ in (4.7) and apply a forward Euler scheme giving

$$\begin{aligned}
&\bar{s}_K^{n+1}\bar{c}_K^{n+1} + \frac{1-\varphi}{\varphi}\rho_{\mathrm{r}} a(\bar{c}_K^{n+1})\\
&\quad = \bar{s}_K^n \bar{c}_K^n + \frac{1-\varphi}{\varphi}\rho_{\mathrm{r}} a(\bar{c}_K^n) - \frac{\Delta t}{\varphi|K|}\sum_{e\subset\partial K}\sum_{i=1}^{q} |e|\omega_i\big(\check{c}_{e,i}\hat{F}_{e,i}^+ + \hat{c}_{e,i}\hat{F}_{e,i}^-\big).
\end{aligned} \tag{5.10}$$

For a given edge $e = K|L$ and each quadrature point $\boldsymbol{x}_i^e$ we can expand the DG solution as

$$c_h\big(\check{\boldsymbol{x}}_i^e, t^n\big) = \bar{c}_K^n + \tilde{c}_{K,L,i}^n \quad \text{and} \quad c_h\big(\hat{\boldsymbol{x}}_i^e, t^n\big) = \bar{c}_L^n + \tilde{c}_{L,K,i}^n \tag{5.11}$$

(using both interior and exterior points), where the terms with tildes indicate a given fluctuation around the elementary averages. Next we denote by $c_{e,i}^{\mathrm{b}} = c^{\mathrm{b}}(\boldsymbol{x}_i^e)$ the vector of predetermined boundary values of the concentration.

The following geometric property is essential for the derivation of the local maximum principle.

LEMMA 5.3. *For any smooth function* $\phi : \mathbb{R}^2 \to \mathbb{R}$ *we have* $\bar{\phi}_K = \phi(\boldsymbol{x}_K) + \mathcal{O}(h_K^2)$*, where* $\boldsymbol{x}_K$ *is the barycenter of* $K \in \mathcal{T}_h$*.*

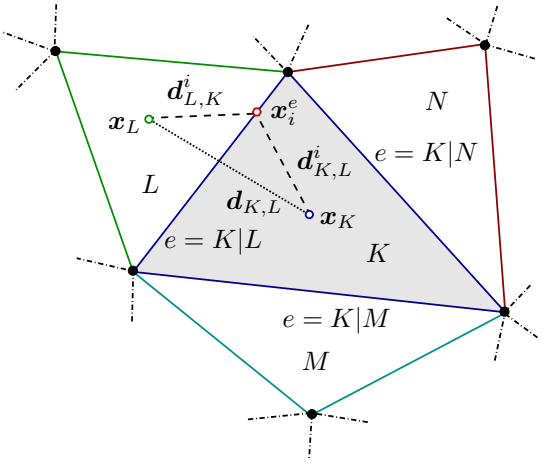

FIG. 1. *Sketch of a given element K and its neighbors L, M, N, in a* **B***-triangulation.*

Proof. As $\boldsymbol{x}_K$ is the barycenter of K, we can write $\boldsymbol{x}_K = \frac{1}{|K|}\int_K \boldsymbol{\xi}\,\mathrm{d}\boldsymbol{\xi}$. Moreover, we can assert that

$$\begin{aligned}\int_K (\boldsymbol{x}-\boldsymbol{x}_K)\cdot\nabla\phi(\boldsymbol{x}_K)\,\mathrm{d}\boldsymbol{x} &= \int_K \left(\boldsymbol{x} - \frac{1}{|K|}\int_K \boldsymbol{\xi}\,\mathrm{d}\boldsymbol{\xi}\right)\cdot\nabla\phi(\boldsymbol{x}_K)\,\mathrm{d}\boldsymbol{x}\\ &= \int_K \boldsymbol{x}\cdot\nabla\phi(\boldsymbol{x}_K)\,\mathrm{d}\boldsymbol{x} - \int_K \boldsymbol{\xi}\cdot\nabla\phi(\boldsymbol{x}_K)\,\mathrm{d}\boldsymbol{\xi}\left(\frac{1}{|K|}\int_K 1\,\mathrm{d}\boldsymbol{x}\right)\\ &= \int_K \boldsymbol{x}\cdot\nabla\phi(\boldsymbol{x}_K)\,\mathrm{d}\boldsymbol{x} - \int_K \boldsymbol{\xi}\cdot\nabla\phi(\boldsymbol{x}_K)\,\mathrm{d}\boldsymbol{\xi} = 0.\end{aligned}$$

Utilizing the Taylor expansion $\phi(\boldsymbol{x}) = \phi(\boldsymbol{x}_K) + (\boldsymbol{x}-\boldsymbol{x}_K)\cdot\nabla\phi(\boldsymbol{x}_K) + \mathcal{O}(h_K^2)$ now yields

$$\begin{aligned}\bar{\phi} &:= \frac{1}{|K|}\int_K \phi(\boldsymbol{x})\,\mathrm{d}\boldsymbol{x} = \frac{1}{|K|}\int_K \big(\phi(\boldsymbol{x}_K) + (\boldsymbol{x}-\boldsymbol{x}_K)\cdot\nabla\phi(\boldsymbol{x}_K) + \mathcal{O}(h_K^2)\big)\mathrm{d}\boldsymbol{x}\\ &= \phi(\boldsymbol{x}_K) + \frac{1}{|K|}\int_K (\boldsymbol{x}-\boldsymbol{x}_K)\cdot\nabla\phi(\boldsymbol{x}_K)\,\mathrm{d}\boldsymbol{x} + \mathcal{O}(h_K^2) = \phi(\boldsymbol{x}_K) + \mathcal{O}(h_K^2).\end{aligned}$$

This completes the proof. ∎

In addition, we require the concept of **B**-triangulations [13], defined in what follows, where for the sake of simplicity, for any edge lying on $\partial\Omega$ its adjacent element will be treated as a ghost cell.

Let $\boldsymbol{x}_K$ and $\boldsymbol{x}_L$ denote the barycenter of K and L, respectively, and $\boldsymbol{x}_e$ denote the midpoint of the edge e (see Figure 1). For $K \in \mathcal{T}_h$ we denote

$$\boldsymbol{d}_{K,L} := \begin{cases}\boldsymbol{x}_e - \boldsymbol{x}_K & \text{if } L \text{ is a ghost cell,}\\ \boldsymbol{x}_L - \boldsymbol{x}_K & \text{otherwise.}\end{cases} \tag{5.12}$$

We identify the segments $\boldsymbol{d}^i_{K,L} = \boldsymbol{x}^e_i - \boldsymbol{x}_K$ for all $e = K|L$, and recall the following definitions from [13].

DEFINITION 5.1. *A mesh $\mathcal{T}_h$ is called a* **B***-triangulation if for any $K \in \mathcal{T}_h$ and pairs $\boldsymbol{d}^i_{K,L}, \boldsymbol{d}^i_{L,K}$, where $i = 1, \ldots, q$ is an index of the quadrature points, one can*

choose segments $\boldsymbol{d}_{K,M}$ *and* $\boldsymbol{d}_{K,N}$ *(defined in* (5.12) *where* $M, N \in \mathcal{N}_K$*) such that*

$$-\boldsymbol{d}^i_{K,L} = \theta^i_{K,L,M}\boldsymbol{d}_{K,M} + \theta^i_{K,L,N}\boldsymbol{d}_{K,N}, \quad \boldsymbol{d}^i_{L,K} = \vartheta^i_{L,K,M}\boldsymbol{d}_{K,M} + \vartheta^i_{L,K,N}\boldsymbol{d}_{K,N}$$

for some nonnegative constants $\theta^i_{K,L,M}, \theta^i_{K,L,N}, \vartheta^i_{L,K,M}$, *and* $\vartheta^i_{L,K,N}$.

DEFINITION 5.2. *A family of triangulations* $\{\mathcal{T}_h\}_{h>0}$ *is called* **B***-uniform if each triangulation* $\mathcal{T}_h$ *is a* **B***-triangulation, and if there exists a constant* $\nu > 0$ *such that*

$$\forall K \in \mathcal{T}_h,\ h > 0 :\ \forall L, M, N \in \mathcal{N}_K :\ \forall i = 1, \dots, q :$$
$$\theta^i_{K,L,M}, \theta^i_{K,L,N}, \vartheta^i_{L,K,M}, \vartheta^i_{L,K,N} \in [0, \nu].$$

The constant ν depends on the choice of $\{\mathcal{T}_h\}_{h>0}$. For acute angle triangles, the existence of such a ν can be verified and the following result holds (see [13]).

LEMMA 5.4. *If* $\mathcal{F}$ *is a family of meshes consisting of acute triangles, then it is* **B***-uniform with constant* $\nu = 2\sigma^3(1+\sigma^2)^{3/2}$, *where* σ *is as in* (3.2).

Going back to our numerical scheme we present a useful result (provided in [13, (2.14)] without proof), and we postpone the proof to the appendix.

LEMMA 5.5. *If* c_h *is a smooth function in a region containing* K *and its neighboring triangles, then*

$$-\tilde{c}^n_{K,L,i} = \theta^i_{K,L,M}\Delta_{K,M} + \theta^i_{K,L,N}\Delta_{K,N} + \mathcal{O}(h^2), \tag{5.13}$$

$$\tilde{c}^n_{L,K,i} = \vartheta^i_{L,K,M}\Delta_{K,M} + \vartheta^i_{L,K,N}\Delta_{K,N} + \mathcal{O}(h^2), \tag{5.14}$$

where we define

$$\Delta_{K,M} := \begin{cases} \Delta_{K,e} & \text{if } e = K|M \subset \partial K \cap \partial\Omega, \\ \bar{c}^n_M - \bar{c}^n_K & \text{otherwise,} \end{cases}$$

$$\Delta_{K,N} := \begin{cases} \Delta_{K,e} & \text{if } e = K|N \subset \partial K \cap \partial\Omega, \\ \bar{c}^n_N - \bar{c}^n_K & \text{otherwise,} \end{cases}$$

and $\Delta_{K,e} = \bar{c}^n_e - \bar{c}^n_K$, *where* $\bar{c}^{\mathrm{b}}_e := \frac{1}{|e|}\int_e c^{\mathrm{b}}\,\mathrm{d}s$. *The quantities* $\theta^i_{K,L,M}$, $\theta^i_{K,L,N}$, $\vartheta^i_{L,K,M}$, *and* $\vartheta^i_{L,K,N}$ *are as in Definition* 5.1.

Lemma 5.5 indicates that for a suitable choice of $\kappa \geq 1$ we can ensure that

$$\tilde{c}^n_{K,L,i} \in I(0, \kappa\mathcal{C}_{K,L,i}), \quad \tilde{c}^n_{L,K,i} \in I(0, \kappa\mathcal{C}_{L,K,i}), \tag{5.15}$$

where

$$\mathcal{C}_{K,L,i} = -(\theta^i_{K,L,M}\Delta_{K,M} + \theta^i_{K,L,N}\Delta_{K,N}),$$
$$\mathcal{C}_{L,K,i} = \vartheta^i_{L,K,M}\Delta_{K,M} + \vartheta^i_{L,K,N}\Delta_{K,N},$$

and where for finitely many numbers $a_1, \dots, a_J$, the interval I is

$$I(a_1, \dots, a_J) := [\min\{a_1, \dots, a_J\}, \max\{a_1, \dots, a_J\}].$$

Note that in the regions where c_h is smooth, conditions (5.15) are satisfied as a consequence of Lemma 5.5. However, if the solution is discontinuous then we require a projection operator $\Lambda\Pi_h$ (defined in [13] for the class of **B**-triangulations), which, in particular, does not compromise the initial order of accuracy, that is, the expected order of accuracy for smooth solutions.

DEFINITION 5.3 (cf. [13]). *The quantity $\Lambda\Pi_h(c_h)|_K$ is defined as the projection by $\Lambda\Pi_h : V_h \to V_h$ of $c_h|_K$ into the nonempty convex set*

$$Q(K, c_h) := \big\{\varphi : \Omega \to \mathbb{R} \mid \varphi|_K \in \mathbb{P}_k(K),\ \bar{\varphi} = \bar{c}_h,\ \textit{and (5.15) holds}\big\}.$$

LEMMA 5.6. *If c_h is computed on a* **B***-uniform family, then*

$$\begin{aligned} -\tilde{c}^n_{K,L,i} &= \kappa\kappa^i_{K,L}\big(\theta^i_{K,L,M}\Delta_{K,M} + \theta^i_{K,L,N}\Delta_{K,N}\big),\\ \tilde{c}^n_{L,K,i} &= \kappa\kappa^i_{L,K}\big(\vartheta^i_{L,K,M}\Delta_{K,M} + \vartheta^i_{L,K,N}\Delta_{K,N}\big), \end{aligned} \tag{5.16}$$

where $\Delta_{K,M}$, $\Delta_{K,N}$, and the constants θ^i and ϑ^i are as in Definition 5.1 *and Lemma* 5.5*, and $0 \le \kappa^i \le 1$.*

Proof. On a **B**-uniform family of triangulation, in the region where c_h is smooth we have the following expression, through Lemma 5.5,

$$\begin{aligned} -\tilde{c}^n_{K,L,i} &= \theta^i_{K,L,M}\Delta_{K,M} + \theta^i_{K,L,N}\Delta_{K,N} + \mathcal{O}(h^2),\\ \tilde{c}^n_{L,K,i} &= \vartheta^i_{L,K,M}\Delta_{K,M} + \vartheta^i_{L,K,N}\Delta_{K,N} + \mathcal{O}(h^2). \end{aligned}$$

Further, from (5.15) we have $\tilde{c}^n_{K,L,i} \in I(0, \kappa\mathcal{C}_{K,L,i})$ and $\tilde{c}^n_{L,K,i} \in I(0, \kappa\mathcal{C}_{L,K,i})$, hence, we can choose constants $0 \le \kappa^i_{K,L}, \kappa^i_{L,K} \le 1$ such that (5.16) holds. In the region where c_h is not smooth, the projection operator provides the expressions (5.16). This completes the proof. ∎

Remark 5.1. Note that by Definition 5.2, the quantities θ^i, ϑ^i in expression (5.16) assume values in $[0, \nu]$. For simplicity we absorb the constants $\kappa\kappa^i_{K,L}$ and $\kappa\kappa^i_{L,K}$ into the quantities $\theta^i_{K,L,M}, \theta^i_{K,L,N}, \vartheta^i_{L,K,M}$, and $\vartheta^i_{L,K,N}$ in (5.16). Consequently the expressions in (5.16) assume the following form, where $\theta^i, \vartheta^i \in [0, \kappa\nu]$:

$$\begin{aligned} -\tilde{c}^n_{K,L,i} &= \theta^i_{K,L,M}\Delta_{K,M} + \theta^i_{K,L,N}\Delta_{K,N},\\ \tilde{c}^n_{L,K,i} &= \vartheta^i_{L,K,M}\Delta_{K,M} + \vartheta^i_{L,K,N}\Delta_{K,N}. \end{aligned}$$

We are now in position to state the local maximum principle for c_h.

THEOREM 5.2. *Let c_h be the discrete concentration resulting from* (4.6)*, advanced in time using the forward Euler scheme on a* **B***-uniform triangulation together with the projection in Definition* 5.3*. Then*

$$\bar{c}^{n+1}_K \in I\big(\bar{c}^n_K;\, \bar{c}^n_L : L \in \mathcal{N}_K;\, \bar{c}^{\mathrm{b}}_e, c^{\mathrm{b}}_{e,1}, \dots, c^{\mathrm{b}}_{e,q} : e \subset \partial K \cap \partial\Omega\big) \quad \forall K \in \mathcal{T}_h, \tag{5.17}$$

provided that $\omega_i \ge 0$ for all i, and

$$\mathrm{cfl} := \Delta t \sup_{e \subset \partial K : K \in \mathcal{T}_h} \frac{|e|}{\varphi|K|} S \le \frac{1}{5 + 34\kappa\nu}, \tag{5.18}$$

where

$$S = \sup_{s \in [0,1]} \left\{ \frac{\partial F_1}{\partial s}, \frac{\partial F_2}{\partial s}, F_1\left(s + \frac{1-\varphi}{\varphi}\rho_{\mathrm{r}} a'\right)^{-1}, F_2\left(s + \frac{1-\varphi}{\varphi}\rho_{\mathrm{r}} a'\right)^{-1} \right\}.$$

Proof. Adding and subtracting $\bar{s}^{n+1}_K \bar{c}^n_K$ in (5.10) and rearranging terms gives

$$\begin{aligned} &\left(\bar{s}^{n+1}_K + \frac{1-\varphi}{\varphi}\rho_{\mathrm{r}} a'(\xi_K)\right)(\bar{c}^{n+1}_K - \bar{c}^n_K) + \bar{c}^n_K(\bar{s}^{n+1}_K - \bar{s}^n_K)\\ &\qquad = -\frac{\Delta t}{\varphi|K|} \sum_{e \subset \partial K} \sum_{i=1}^{q} |e| \omega_i \big(\check{c}_{e,i}\hat{F}^+_{e,i} + \hat{c}_{e,i}\hat{F}^-_{e,i}\big), \end{aligned}$$

where

$$a'(\xi_K) = \frac{a(\bar{c}_K^{n+1}) - a(\bar{c}_K^n)}{\bar{c}_K^{n+1} - \bar{c}_K^n} \quad \text{for some point } \xi_K \text{ between } \bar{c}_K^{n+1} \text{ and } \bar{c}_K^n.$$

We then replace $\bar{s}_K^{n+1} - \bar{s}_K^n$ by (5.1), leading to

$$\left(\bar{s}_K^{n+1} + \frac{1-\varphi}{\varphi}\rho_{\mathrm{r}} a'(\xi_K)\right)(\bar{c}_K^{n+1} - \bar{c}_K^n) + \bar{c}_K^n\left(-\frac{\Delta t}{\varphi|K|}\sum_{e\subset\partial K}\sum_{i=1}^{q}\omega_i|e|\big(\hat{F}_{e,i}^{+} + \hat{F}_{e,i}^{-}\big)\right)$$
$$= -\frac{\Delta t}{\varphi|K|}\sum_{e\subset\partial K}\sum_{i=1}^{q}|e|\omega_i\big(\check{c}_{e,i}\hat{F}_{e,i}^{+} + \hat{c}_{e,i}\hat{F}_{e,i}^{-}\big),$$

which can be written as

$$\bar{c}_K^{n+1} = \bar{c}_K^n - \frac{\Delta t}{\varsigma_K\varphi|K|}\sum_{e\in\partial K}\sum_{i=1}^{q}|e|\omega_i\big(\hat{F}_{e,i}^{+}(\check{c}_{e,i} - \bar{c}_K^n) + \hat{F}_{e,i}^{-}(\hat{c}_{e,i} - \bar{c}_K^n)\big), \tag{5.19}$$

where $\varsigma_K := \bar{s}_K^{n+1} + (1-\varphi)\varphi^{-1}\rho_{\mathrm{r}}a'(\xi_K) > 0$, since $\bar{s}_K^n \in [0,1]$ and $a' > 0$.

In what follows, for a given K we let $\mathcal{A} := \partial K \cap \partial\Omega$ and $\mathcal{B} := \partial K \setminus \partial\Omega$. Considering also the boundary terms, and using (5.11), we then obtain from relation (5.19)

$$\begin{aligned}\bar{c}_K^{n+1} = \bar{c}_K^n &+ \Delta t\sum_{e=K|L\subset\mathcal{B}}\sum_{i=1}^{q}\big(\eta_{e,i}^{+}(-\tilde{c}_{K,L,i}^n) + \eta_{e,i}^{-}(\tilde{c}_{L,K,i}^n + \bar{c}_L^n - \bar{c}_K^n)\big)\\ &+ \Delta t\sum_{e\subset\mathcal{A}}\sum_{i=1}^{q}\big(\eta_{e,i}^{+}(-\tilde{c}_{K,e,i}^n) + \eta_{e,i}^{-}(c_{e,i}^b - \bar{c}_K^n)\big),\end{aligned} \tag{5.20}$$

where

$$\eta_{e,i}^{+} = \frac{|e|\omega_i\hat{F}_{e,i}^{+}}{\varsigma_K\varphi|K|} \geq 0, \quad \eta_{e,i}^{-} = -\frac{|e|\omega_i\hat{F}_{e,i}^{-}}{\varsigma_K\varphi|K|} \geq 0.$$

Then Lemma 5.6 together with Remark 5.1 allows us to write

$$-\tilde{c}_{K,L,i}^n = \sum_{N\in\mathcal{N}_K\setminus\{L\}}\theta_{K,L,N}^i(\Delta_{K,N}) + \sum_{d\subset\mathcal{A}}\theta_{K,L,d}^i(\Delta_{K,d}),$$
$$\tilde{c}_{L,K,i}^n = \sum_{N\in\mathcal{N}_K\setminus\{L\}}\vartheta_{L,K,N}^i(\Delta_{K,N}) + \sum_{d\subset\mathcal{A}}\vartheta_{L,K,d}^i(\Delta_{K,d}),$$

where $\theta_{K,L,N}^i, \vartheta_{L,K,N}^i, \theta_{K,L,d}^i, \vartheta_{L,K,d}^i \geq 0$. Inserting these values into (5.20) leads to

$$\begin{aligned}\bar{c}_K^{n+1} = \bar{c}_K^n &+ \Delta t\sum_{N\in\mathcal{N}_K}\Theta_{K,N}(\Delta_{K,N}) + \Delta t\sum_{d\subset\mathcal{A}}\Theta_{K,d}(\Delta_{K,d})\\ &+ \Delta t\sum_{d\subset\mathcal{A}}\sum_{i=1}^{q}\eta_{d,i}^{-}(c_{d,i}^b - \bar{c}_K^n)\end{aligned} \tag{5.21}$$

with

$$\Theta_{K,N} := \sum_{\substack{e=K|L\subset\mathcal{B}\\ L\neq N}}\sum_{i=1}^{q}(\eta_{e,i}^{+}\theta_{K,L,N}^i + \eta_{e,i}^{-}\vartheta_{L,K,N}^i) + \sum_{d\subset\mathcal{A}}\sum_{i=1}^{q}\eta_{d,i}^{+}\theta_{K,d,N}^i + \sum_{i=1}^{q}\eta_{e_N,i}^{-},$$

$$\Theta_{K,d} := \sum_{e=K|L\subset\mathcal{B}}\sum_{i=1}^{q}(\eta_{e,i}^{+}\theta_{K,L,d}^i + \eta_{e,i}^{-}\vartheta_{L,K,d}^i) + \sum_{\sigma\subset\mathcal{A}}\sum_{i=1}^{q}\eta_{\sigma,i}^{+}\theta_{K,\sigma,d}^i,$$

where $e_N = K|N$. Should one be able to obtain a bound for Δt, valid whenever (5.18) holds and $\omega_i \geq 0$ for all i, then a direct application of (5.21) would imply (5.17) and the desired result would follow. Let us then concentrate in deriving such a bound.

Let us first define

$$\Upsilon_K := \Delta t \left(\sum_{N \in \mathcal{N}_K} \Theta_{K,N} + \sum_{d \subset \mathcal{A}} \Theta_{K,d} + \sum_{d \subset \mathcal{A}} \sum_{i=1}^{q} \eta_{d,i}^{-} \right). \tag{5.22}$$

We can now write

$$\begin{aligned}
\Upsilon_K = \Delta t \Bigg(& \sum_{N \in \mathcal{N}_K} \Bigg\{ \sum_{\substack{e=K|L \subset \mathcal{B} \\ L \neq N \\ i=1,\dots,q}} (\eta_{e,i}^{+} \theta_{K,L,N}^{i} + \eta_{e,i}^{-} \vartheta_{L,K,N}^{i}) + \sum_{\substack{d \subset \mathcal{A} \\ i=1,\dots,q}} \eta_{d,i}^{+} \theta_{K,d,N}^{i} + \sum_{i=1}^{q} \eta_{e_N,i}^{-} \Bigg\} \\
& + \sum_{d \subset \mathcal{A}} \Bigg\{ \sum_{\substack{e=K|L \subset \mathcal{B} \\ i=1,\dots,q}} (\eta_{e,i}^{+} \theta_{K,L,d}^{i} + \eta_{e,i}^{-} \vartheta_{L,K,d}^{i}) + \sum_{\substack{\sigma \subset \mathcal{A} \\ i=1,\dots,q}} \eta_{\sigma,i}^{+} \theta_{K,\sigma,d}^{i} \Bigg\} + \sum_{\substack{d \subset \mathcal{A} \\ i=1,\dots,q}} \eta_{d,i}^{-} \Bigg) \\
\leq \mathrm{cfl} \Bigg(& \sum_{N \in \mathcal{N}_K} \Bigg\{ \sum_{\substack{e=K|L \subset \mathcal{B} \\ L \neq N \\ i=1,\dots,q}} \omega_i (\theta_{K,L,N}^{i} + \vartheta_{L,K,N}^{i}) + \sum_{\substack{d \subset \mathcal{A} \\ i=1,\dots,q}} \omega_i \theta_{K,d,N}^{i} + \sum_{i=1}^{q} \omega_i \Bigg\} \\
& + \sum_{d \subset \mathcal{A}} \Bigg\{ \sum_{\substack{e=K|L \subset \mathcal{B} \\ i=1,\dots,q}} \omega_i (\theta_{K,L,d}^{i} + \vartheta_{L,K,d}^{i}) + \sum_{\substack{\sigma \subset \mathcal{A} \\ i=1,\dots,q}} \omega_i \theta_{K,\sigma,d}^{i} \Bigg\} + \sum_{\substack{d \subset \mathcal{A} \\ i=1,\dots,q}} \omega_i \Bigg).
\end{aligned}$$

Finally, noting that $\sum_i \omega_i = 1$, we obtain

$$\begin{aligned}
\Upsilon_K & \leq \mathrm{cfl} \Bigg(\sum_{\substack{e=K|L \subset \mathcal{B} \\ i=1,\dots,q}} \omega_i 2\kappa\nu \sum_{N \in \mathcal{N}_K \setminus \{L\}} 1 + \sum_{\substack{d \subset \mathcal{A} \\ i=1,\dots,q}} \omega_i \kappa\nu \sum_{N \in \mathcal{N}_K} 1 + \sum_{N \in \mathcal{N}_K} 1 \\
& \qquad + \sum_{\substack{e=K|L \subset \mathcal{B} \\ i=1,\dots,q}} \omega_i 2\kappa\nu \sum_{d \subset \mathcal{A}} 1 + \sum_{\substack{\sigma \subset \mathcal{A} \\ i=1,\dots,q}} \omega_i \kappa\nu \sum_{d \subset \mathcal{A}} 1 + \sum_{d \subset \mathcal{A}} 1 \Bigg) \\
& \leq \mathrm{cfl} \Bigg(\sum_{e=K|L \subset \mathcal{B}} 4\kappa\nu + \sum_{e \subset \mathcal{A}} 3\kappa\nu + 3 + \sum_{e=K|L \subset \mathcal{B}} 4\kappa\nu + \sum_{e \subset \mathcal{A}} 2\kappa\nu + 2 \Bigg) \\
& \leq \mathrm{cfl}(12\kappa\nu + 6\kappa\nu + 3 + 12\kappa\nu + 4\kappa\nu + 2) \leq 1.
\end{aligned}$$

Then, from (5.22) we readily obtain a bound for the time step. ∎

6. Numerical results. Before presenting the numerical tests, we recall that the interaction between the flow and transport solvers is realized using a classical iterative coupling (or sequential strategy). Starting from an initial distribution of saturation and concentrations, one solves first (1.3) for velocity and pressure, followed by a saturation/concentrations solution which comprises an inner iteration loop to reduce the nonlinear residuals associated with the adsorption term. The Newton algorithm uses a relative tolerance of 10^{-5}. Additional fixed-point iterations of the local-in-time coupling are performed until a prescribed stopping criterion is met (based on the discrete ℓ^∞-norm of the residuals and a tolerance of 10^{-6}), and then the algorithm advances to the next time step. In practice, no more than three Picard steps are

TABLE 1
Test 1A: *convergence history for the* $\mathbf{H}(\mathrm{div})$*-conforming DG method for the Brinkman flow equations using a* $\mathbb{BDM}_1$-$\mathbb{P}_0$ *approximation of velocity and pressure.*

Degrees of freedom	h	$e_0(\boldsymbol{u})$	rate	$e_h(\boldsymbol{u})$	rate	$e_h(p)$	rate
84	0.4714	0.8044	–	6.8137	–	2.9578	–
220	0.2828	0.3443	1.8014	3.8800	0.8916	1.4863	0.9394
684	0.1571	0.1129	1.8522	2.2360	0.9376	0.6668	1.3638
2380	0.0832	0.0367	1.8996	1.1969	0.9827	0.2358	1.4343
8844	0.0429	0.0108	1.9239	0.6209	0.9896	0.1122	1.1202
34060	0.0218	0.0031	1.9711	0.3205	0.9853	0.0612	0.9854
133607	0.0110	0.0009	1.9821	0.1614	0.9864	0.0368	0.9918
529458	0.0055	0.0003	1.9944	0.0734	0.9933	0.0181	0.9985

required. We stress that a monolithic Newton solve for saturation and concentrations is in principle not appropriate as the tangent problem is not well defined due to the discontinuity of the nonlinear fluxes coupling s_h and $\boldsymbol{c}_h$. Numerical evidence of this phenomenon (which manifests itself as spurious solutions generated from linearizing the flux functions) has been reported in the literature [26, experiments 2 and 3]. As we will observe below, these effects are not encountered in any of our simulations. All linear solves in this section, including those inside the Newton steps, are performed using the distributed supernodal LU method [15].

6.1. Spatio-temporal accuracy of transport and flow approximations (Tests 1A–1C). In our first set of examples, we study the accuracy of the flow and transport solvers separately. First, regarding the flow approximation, if we assume a constant saturation and polymer concentration, we can construct the closed-form solution for the steady Brinkman problem

$$\boldsymbol{u}(x,y) = \begin{pmatrix} -256x^2(x-1)^2y(y-1)(2y-1) \\ 256y^2(y-1)^2x(x-1)(2x-1) \end{pmatrix}, \qquad p(x,y) = \left(x-\frac{1}{2}\right)\left(y-\frac{1}{2}\right) \tag{6.1}$$

defined on the unit disk. Permeability and viscosity take constant values $\kappa = \mu = 1$, and $\boldsymbol{g}$ is constructed inserting (6.1) into the momentum equation (1.3). We choose the stabilization parameter $\alpha = 2\times 10^5$ and the mean value of the pressure approximation is fixed to zero using a real Lagrange multiplier. The convergence history associated with the scheme (3.3) is portrayed in Table 1, showing optimal convergence rates (of $O(h)$) measured in the energy norms (3.4).

Second, the accuracy of the approximate transport problem in the case of smooth coefficients and regular solutions can be assessed through a convergence history generated using the following exact solution

$$s = \cos^2(\pi x)\cos^2(\pi y)\exp(-t),\ \ c_l = 0.2l^2 + 0.025l\sin^2(\pi x)\sin^2(\pi y)\exp(-t)$$

for $l = 1, 2$ and defined on the unit disk, for $t \in [0, 1]$. A known velocity of the mixture is assumed: $\boldsymbol{u} = (\sin(\pi x)\cos(\pi y), -\cos(\pi x)\sin(\pi y))^{\mathrm{T}}\sin(t)$, and a set of adimensional parameters and nonlinear model functions closing the system is given by $f(s,\boldsymbol{c}) = s^2[s^2 + (1-s)^2(0.5 + 10c_1 + 5c_2)]^{-1}$, $a_l(c_l) = c_l(5 + 5c_l)^{-1}$, $k_{\mathrm{rw}} = s^2$, $k_{\mathrm{rn}} = (1-s)^2$, $\varphi = 1$, $\mu_{\mathrm{w}}(c_1, c_2) = \mu_{\mathrm{w},0} + \mu_{\mathrm{w},0}(c_1 + c_2)$, $\mu_{\mathrm{w},0} = 0.1$, $\mu_{\mathrm{n}} = 1$, and $\kappa = 1$.

To assess the convergence properties of the spatial DG discretization, we choose a fine time step $\Delta t = 10^{-3}$ and partition Ω into a sequence of eight successively refined meshes and measure errors in the energy norm for piecewise linear and piecewise

TABLE 2

Test 1B: *convergence history for the* **H**(div)*-conforming DG method (using piecewise linear and piecewise quadratic elements) for the transport equations. Errors are measured in the broken* H^1*-norm.*

Degrees of freedom	h	$e(s)$	rate	$e(c_1)$	rate	$e(c_2)$	rate
			($k = 1$)				
18	2.0000	2.3284	–	0.7835	–	0.5116	–
54	1.0000	1.1266	0.9798	0.2998	1.3857	0.1415	1.1951
162	0.8854	0.9411	1.0778	0.1753	0.9514	0.0720	0.8478
558	0.5000	0.3521	1.0204	0.1275	1.0413	0.0361	0.9681
1890	0.2848	0.1258	1.0284	0.0961	0.9525	0.0196	0.9862
6732	0.1489	0.0406	1.0455	0.0584	0.9616	0.0101	0.9752
26946	0.0770	0.0215	0.9574	0.0301	0.9884	0.0060	0.9641
104634	0.0427	0.0153	0.9502	0.0188	0.9463	0.0032	0.9547
			($k = 2$)				
36	2.0000	1.4722	–	0.4025	–	0.2599	–
108	1.0000	0.8280	1.4112	0.1832	1.5648	0.1258	1.8019
324	0.8854	0.2322	1.9733	0.0614	1.9634	0.0438	1.4250
1116	0.5000	0.1266	1.8991	0.0175	1.8773	0.0162	1.9081
3780	0.2848	0.0403	1.9802	0.0048	1.9678	0.0042	1.8655
13464	0.1489	0.0161	1.9753	0.0013	1.9471	0.0011	1.6568
53892	0.0770	0.0054	1.9276	0.0004	1.8612	0.0004	1.9523
209268	0.0427	0.0015	1.7427	0.0001	1.8951	0.0001	2.0091

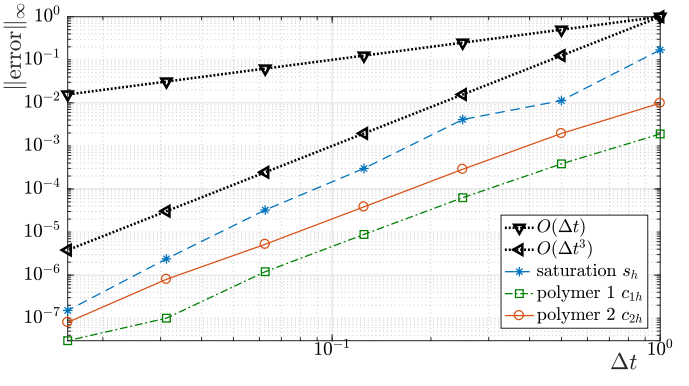

FIG. 2. *Test* 1C: *error history associated with the time discretization of the coupled system using an SSP-RK method of order* 3.

quadratic approximations (i.e., $k = 1, 2$), computed at final time $t = 1$. Table 2 indicates that the method achieves an asymptotic $O(h^k)$ convergence. The accuracy of the temporal optimal SSP-RK scheme (explicitly, of three stages and of third order, using an effective SSP coefficient of 1/3) is studied by setting a fine-resolution space discretization with $h = 2^{-7}$ and successively refine the time interval on seven levels. For these smooth solutions, an optimal convergence order of $O(\Delta t^3)$ is obtained when measuring errors in the $\ell^\infty(H^1)$-norm at $t = 0.5$, as presented in Figure 2. The use of more RK stages will produce smaller errors, but the convergence order will remain the same.

6.2. Water-oil system (Test 2). With the aim of testing the suitability of the method in the presence of rough coefficients and when sharp features are expected in the solution, let us now consider the infiltration of water into oil, first without the

action of polymers, that is, we set $\boldsymbol{c} \equiv \mathbf{0}$. We conduct a classical simulation on a porous box $\Omega = (0, 1.4) \times (0, 1)$, with constant porosity $\varphi = 0.35$ and having an idealized winding crack of sinusoidal shape, characterized by the intrinsic permeability $\kappa(x, y) = \max\{\exp(-10y+5+\sin(10x))^2, 0.01\}$. We employ the mildly nonlinear Brooks–Corey relative permeabilities $k_{\mathrm{rw}} = s^2$, $k_{\mathrm{rn}} = (1-s)^2$, so the mobilities and fractional flow function (of the wetting phase) depend only on the water saturation. No gravity effects are taken into account, and the remaining model parameters are set as $\mu_{\mathrm{w}} = 0.25$ and $\mu_{\mathrm{n}} = 1$. We construct an unstructured triangular mesh of 45360 elements, and at each time iteration, the time step is determined from a CFL condition, which in this case produces an average step of $\Delta t = 5 \times 10^{-4}$. The stabilization parameter used here is $\alpha = 10^3$. The porous block is initially full of oil (that is, $s = 0$) and a constant profile of water ($s = 1$) is imposed on the left wall (which is the inflow boundary), a linear pressure profile $p_0(x, y) = (1.4 - x)/1.4$ is imposed on the whole boundary (and actually implemented as a natural boundary condition, with an additional term $-\langle p_0, \boldsymbol{v}_h \cdot \boldsymbol{n}\rangle_{\partial\Omega}$ appearing as part of the right-hand side $\mathcal{F}^s$ of the weak formulation (3.3)), and the velocity is not prescribed. It is stressed that a careful treatment of the numerical flux at the inflow boundary is essential to actually onset the injection of water into the domain. The system is evolved for about 1000 time steps, and we collect the numerical results in Figure 3. Isocontours of each individual field are displayed at two time instants, showing the expected advance of the water front following the preferential path marked by the winding crack, and high velocity gradients on the region of large permeabilities.

6.3. Polymer flooding of an idealized reservoir (Test 3). We now turn to the simulation of polymer flooding of an oil reservoir, where the full model specified in section 2 is relevant. We consider $\mathcal{M} = 1$ and model parameters together with constitutive relationships (modified from those in [39]) are taken as follows: $a(c) = c_{\max}\frac{a_0 c}{1+a_0 c}$, $\mu_{\mathrm{w}}(c) = \mu_{\mathrm{w},0} + 0.75\mu_{\mathrm{w},0}c_{\max}^{-1}c$, $\rho_{\mathrm{w}} = 1$, $\rho_{\mathrm{n}} = 0.58$, $\mu_{\mathrm{w},0} = 0.35$, $\mu_{\mathrm{n}} = 3.5$, $\varphi = 0.25$, $a_0 = 0.1$, $\lambda_{\mathrm{w}}(s, c) = s^2/\mu_{\mathrm{w}}(c)$, $\lambda_{\mathrm{n}}(s) = (1-s)^2/\mu_{\mathrm{n}}$. The stabilization constant is $\alpha = 1$ and the domain is now the unit square $\Omega = (0, 1)^2$. The permeability distribution is characterized by a nonhomogeneous field where 25 disks of radius 0.005 (having a much lower permeability) are randomly located in the domain. More precisely, we set $\kappa(x, y) = \max(\sum_{i=1}^{25} \exp[-\frac{1}{0.005}\{(x - q_x(i))^2 + (y - q_y(i))^2\}], 0.0001)$, where the random points are $(q_x(i), q_y(i))$. Moreover, the rock porosity is now smaller than in Test 2, $\varphi = 0.2$, the pressure profile imposed on the boundaries is linear, and we now assume that the effect of the external motion of the flow patterns is due to the polymer concentration rather than the water saturation and we regard the obtained simulated scenarios at three different time instants. We consider that the porous slab is initially full of oil and a constant profile of water (that is, $s = 1$) and polymers is injected on the left wall. The domain is divided into 32K triangular elements and from Figure 4 we can observe the differences between the sweeping process (of transporting the oleic phase from the inlet boundary to the outlet) according to the concentration of polymers present at the inlet boundary. We have run two cases that differ only on the amount of polymers injected ($c_{in} = c_{\max} \in \{0.2, 3.2\}$). The numerical results also imply that more oil is displaced in the presence of a higher polymer concentration, but due to gravity the polymers will tend to get retained within the domain.

6.4. Three model extensions (Test 4). As a final example we study a more general constitutive model where three additional components are incorporated: a capillary pressure, a sorption term being only Hölder continuous, and a nonlinear

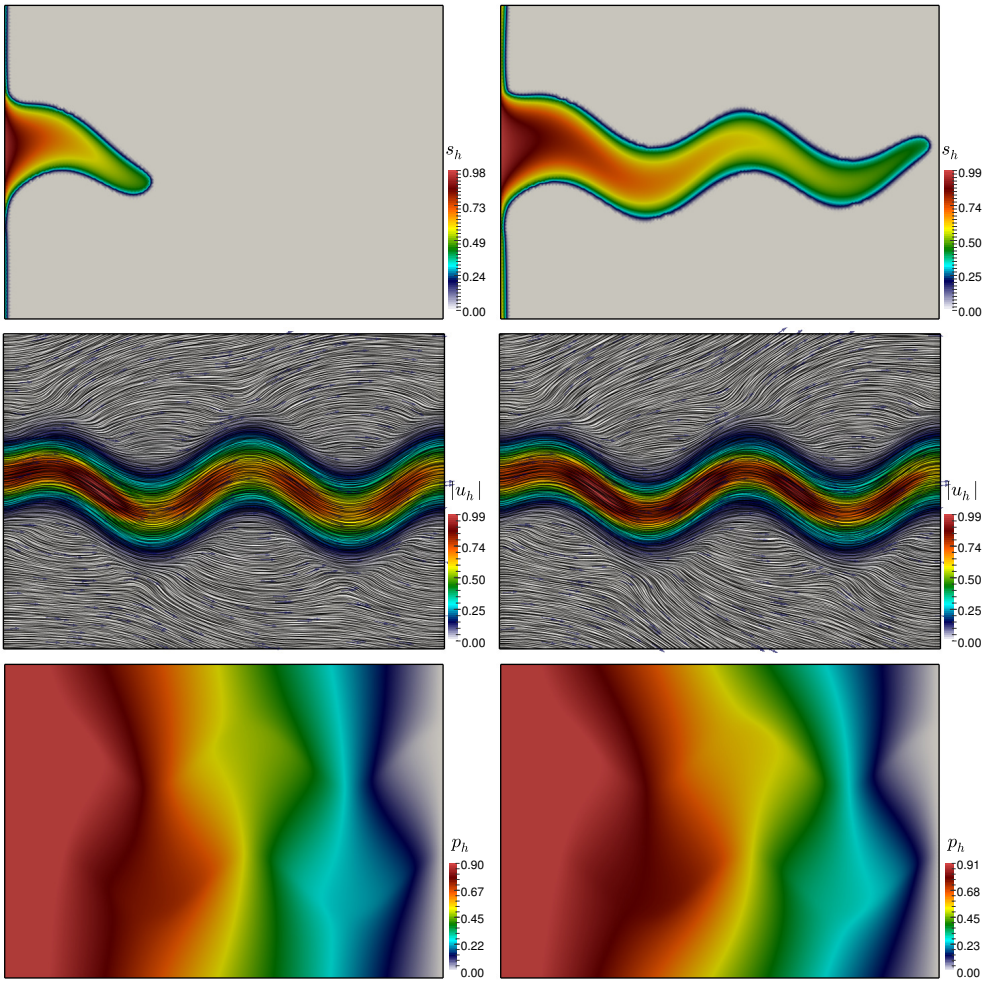

FIG. 3. *Test* 2: *Numerical solution of the water infiltration in porous media computed with an* $\mathbf{H}(\mathrm{div})$*-conforming DG approximation of velocity, and piecewise discontinuous saturation and pressure. Water saturation (top), velocity magnitude (middle), and pressure profiles (bottom) recorded at times* $t = 0.16$ *and* $t = 0.48$ *(left and right panels, respectively).*

concentration dependence for the viscosity. Although these generalizations prevent us from applying directly the stability analysis of section 5, we stress that the principal ingredients of our method (combining $\mathbf{H}(\mathrm{div})$-conforming DG schemes and classical DG schemes and using discontinuous fluxes) are still amenable to solving the extended model addressed in this test.

We consider two kinds of polymers $\mathcal{M} = 2$, and as a modified sorption term we will adopt the Freundlich isotherm defined in (2.1) and specified by the parameters $c_1^{\max} = 0.71, c_2^{\max} = 0.92$, and $\alpha_{\mathrm{F}} = 0.5$. Regarding the viscosity of the water (now assumed partially mixed with the polymers), instead of the linear relation (2.2) we here consider the dependence

$$\mu_{\mathrm{w}}(\boldsymbol{c}) = [\mu_{\mathrm{w},0} + a(c_1 + c_2)]^{1/2}[\mu_{\mathrm{w},0} + a(c_1^{\max} + c_2^{\max})]^{1/2}$$

with $a = 0.25$, adopted from the generalized Todd–Longstaff mixing model used in [18]. As in the previous examples, the relative permeabilities for water and oil

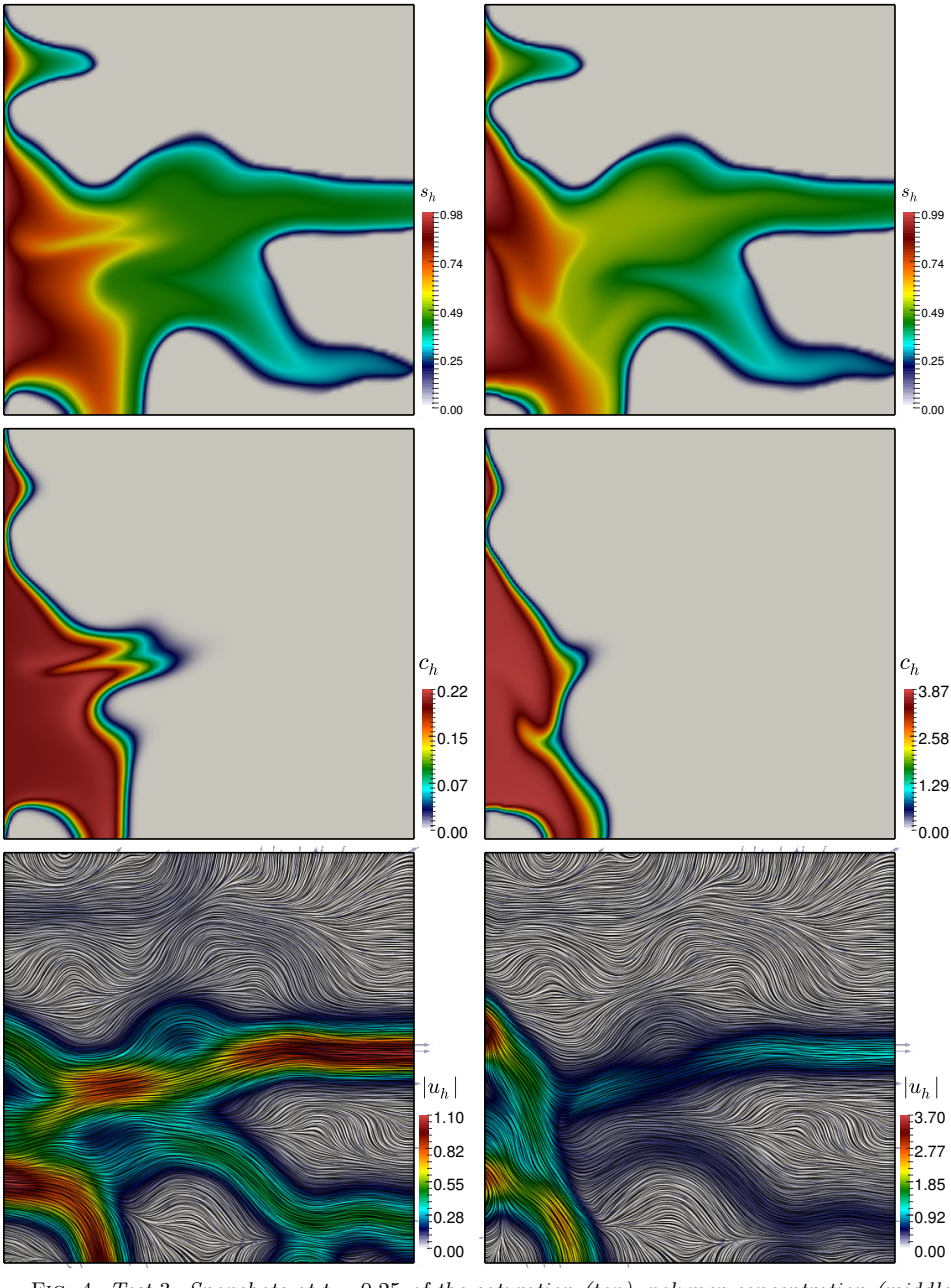

FIG. 4. *Test* 3: *Snapshots at* $t = 0.25$ *of the saturation (top), polymer concentration (middle), and velocity profiles (bottom) obtained according to a low* ($c_{\max} = 0.22$, *left) and high* ($c_{\max} = 3.9$, *right) polymer concentration imposed at the inlet boundary.*

correspond to $k_{\mathrm{rw}} = s^2$ and $k_{\mathrm{rn}} = (1-s)^2$, respectively. The total pressure sought in the Brinkman formulation from section 3 (the Lagrange multiplier enforcing incompressibility) assumes that the individual pressures of each phase coincide. Obviating this restriction, one then has to solve for p_{w} and p_{n}, and an additional equation is required. For this example we include a classical constitutive equation for capillary pressure (that is, the pressure difference between two incompressible fluid phases)

written in terms of water saturation [7]:

$$p_{\mathrm{w}} - p_{\mathrm{n}} = p_c(s) = p_0(1-s)^{1/6.23},$$

where it is assumed that no residual saturation is trapped in the pores. We also notice that the total pressure is $p = sp_{\mathrm{w}} + (1-s)p_{\mathrm{n}}$ and one of the phasic pressures is simply $p_{\mathrm{w}} = p + (1-s)p_c(s)$ (see, e.g., [36]). Other synthetic model constants and coefficients are set as $p_0 = 0.05$, $\varphi = 0.4$, $\rho_{\mathrm{w}} = 1$, $\rho_{\mathrm{n}} = 0.83$, $\mu_{\mathrm{w},0} = 1$, $\mu_{\mathrm{n}} = 7.2$, $\lambda_{\mathrm{w}}(s, \boldsymbol{c}) = s^2/\mu_{\mathrm{w}}(\boldsymbol{c})$, $\lambda_{\mathrm{n}}(s) = (1-s)^2/\mu_{\mathrm{n}}$, and $\alpha = 100$. We disregard gravitational forces. The spatial domain is the rectangular layer $\Omega = (0, 670)\times(0, 300)\mathrm{m}^2$, which we discretize into an unstructured mesh of 45K triangular elements. Soil heterogeneity is incorporated in the isotropic, random logarithmic permeability field $\kappa(\boldsymbol{x})$, characterized by the bounds $\kappa_{\min} = 0.0001$ and $\kappa_{\max} = 9000$, where no apparent connections are observable between the regions of low permeability. This reservoir is initially filled with a homogeneous saturation $s = 0.2$, and we inject a mixture of water and polymers (with $s = 1$, $c_1 = 0.6$, $c_2 = 0.8$) from a well of radius 5 m located at the bottom left corner of the domain, while extraction occurs through a production well on the top right corner. We use a constant time step of $\Delta t = 1.5$ and conduct the simulation until $t = 20000$. Figure 5 contains snapshots of the approximate distribution of water saturation recorded at different times. The profiles of the two injected polymers follow a similar pattern.

6.5. Concluding remark. Note that the numerical results of Tests 2 and 3 (Figures 3 and 4), which are covered by Theorem 5.1, but also those of Test 4 (Figure 5), indicate numerical saturation values s_h indeed assume values in $[0, 1]$ only (where the plotted quantities are the cell averages). Moreover, according to the middle row of Figure 4, the numerical results of Test 3 for c_h remain within the interval $[0, c_{\max}]$ in both cases of $c_{\max} = 0.22$ and $c_{\max} = 3.9$, in agreement with Theorem 5.2.

Appendix: Proof of Lemma 5.5. We present the proofs for (5.13) and (5.14) in the following lines. From (5.11), suppressing the dependence on t^n and using Lemma 5.3, we obtain

$$-\tilde{c}_{K,L,i} = -c_h(\tilde{\boldsymbol{x}}_i^e) + \bar{c}_K = -c_h(\tilde{\boldsymbol{x}}_i^e) + c_h(\boldsymbol{x}_K) + \mathcal{O}(h^2).$$

A Taylor expansion of c_h around $\boldsymbol{x}_K$ now gives

$$\begin{aligned} -\tilde{c}_{K,L,i} &= -(\boldsymbol{x}_i^e - \boldsymbol{x}_K)\cdot\nabla c_h(\boldsymbol{x}_K) + \mathcal{O}(h^2) = -\boldsymbol{d}_{K,L}^i\cdot\nabla c_h(\boldsymbol{x}_K) + \mathcal{O}(h^2) \\ &= (\theta_{K,L,M}^i \boldsymbol{d}_{K,M} + \theta_{K,L,N}^i \boldsymbol{d}_{K,N})\cdot\nabla c_h(\boldsymbol{x}_K) + \mathcal{O}(h^2), \end{aligned} \tag{A.1}$$

and rearranging terms we get

$$\boldsymbol{d}_{K,L}\cdot\nabla c_h(\boldsymbol{x}_K) = (\boldsymbol{x}_L - \boldsymbol{x}_K)\cdot\nabla c_h(\boldsymbol{x}_K) = c_h(\boldsymbol{x}_L) - c_h(\boldsymbol{x}_K) + \mathcal{O}(h^2), \quad L\in\mathcal{N}_K.$$

By Lemma 5.3, $c_h(\boldsymbol{x}_L) = \bar{c}_L + \mathcal{O}(h^2)$ for $L\in\mathcal{N}_K$; consequently,

$$\boldsymbol{d}_{K,L}\cdot\nabla c_h(\boldsymbol{x}_K) = \bar{c}_L - \bar{c}_K + \mathcal{O}(h^2), \quad L\in\mathcal{N}_K.$$

Inserting these values into (A.1) we get

$$\begin{aligned} -\tilde{c}_{K,L,i} &= \theta_{K,L,M}^i(\bar{c}_M - \bar{c}_K + \mathcal{O}(h^2)) + \theta_{K,L,N}^i(\bar{c}_N - \bar{c}_K + \mathcal{O}(h^2)) + \mathcal{O}(h^2), \\ &= \theta_{K,L,M}^i\Delta_{K,M} + \theta_{K,L,N}^i\Delta_{K,N} + \mathcal{O}(h^2), \end{aligned}$$

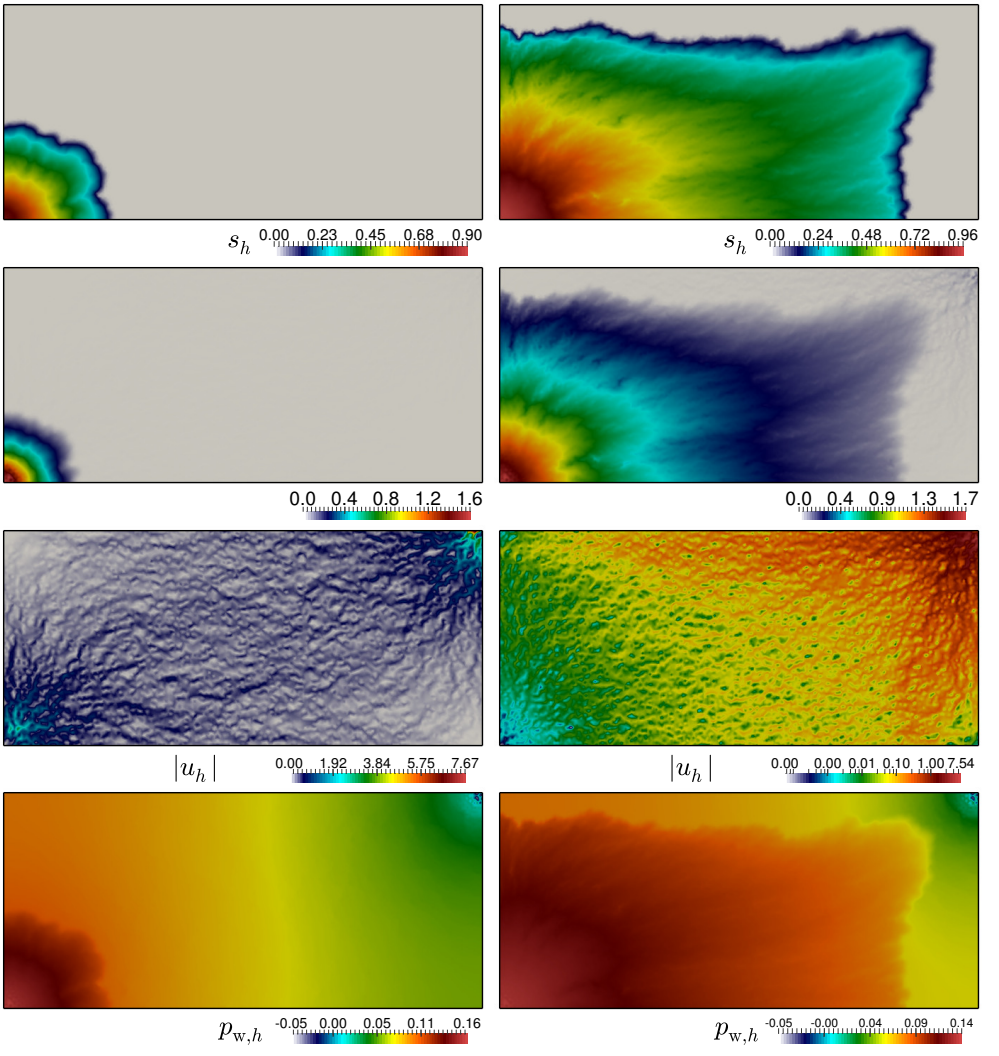

FIG. 5. *Test* 4: *Snapshots at* $t = 100$ *and* $t = 1500$ *(left and right, respectively) of the saturation, total polymer concentration* $(c_{1,h} + c_{2,h})$*, magnitude of the filtration velocity, and water pressure.*

which verifies (5.13). Since c_h is assumed smooth, $c_h(\check{\boldsymbol{x}}_i^e, t^n) = c_h(\hat{\boldsymbol{x}}_i^e, t^n)$. Next, from (5.11) we can use similar arguments as above (namely, a Taylor expansion of c_h around $\boldsymbol{x}_K$ and Lemma 5.3 repeatedly) to obtain

$$\begin{aligned}
\tilde{c}_{L,K,i} &= c_h\big(\hat{\boldsymbol{x}}_i^e, t^n\big) - \bar{c}_L^n = c_h(\boldsymbol{x}_K) + (\boldsymbol{x}_i^e - \boldsymbol{x}_K)\cdot\nabla c_h(\boldsymbol{x}_K) - \bar{c}_L + \mathcal{O}(h^2)\\
&= \bar{c}_K + (\boldsymbol{x}_i^e - \boldsymbol{x}_L + \boldsymbol{x}_L - \boldsymbol{x}_K)\cdot\nabla c_h(\boldsymbol{x}_K) - \bar{c}_L + \mathcal{O}(h^2)\\
&= \bar{c}_K - \bar{c}_L + (c_h(\boldsymbol{x}_L) - c_h(\boldsymbol{x}_K)) + (\boldsymbol{x}_i^e - \boldsymbol{x}_L)\cdot\nabla c_h(\boldsymbol{x}_K) + \mathcal{O}(h^2)\\
&= \bar{c}_K - \bar{c}_L + (\bar{c}_L - \bar{c}_K) + (\boldsymbol{x}_i^e - \boldsymbol{x}_L)\cdot\nabla c_h(\boldsymbol{x}_K) + \mathcal{O}(h^2)\\
&= \vartheta_{L,K,M}^i \boldsymbol{d}_{K,M}\cdot\nabla c_h(\boldsymbol{x}_K) + \vartheta_{L,K,N}^i \boldsymbol{d}_{K,N}\cdot\nabla c_h(\boldsymbol{x}_K) + \mathcal{O}(h^2).
\end{aligned}$$

Using once again the Taylor expansion of c_h around $\boldsymbol{x}_K$ we get

$$\boldsymbol{d}_{K,L}\cdot\nabla c_h(\boldsymbol{x}_K) = (\boldsymbol{x}_L - \boldsymbol{x}_K)\cdot\nabla c_h(\boldsymbol{x}_K) = c_h(\boldsymbol{x}_L) - c_h(\boldsymbol{x}_K) + \mathcal{O}(h^2), \quad L \in \mathcal{N}_K,$$

and as before, $\boldsymbol{d}_{K,L} \cdot \nabla c_h(\boldsymbol{x}_K) = \bar{c}_L - \bar{c}_K + \mathcal{O}(h^2)$ for $L \in \mathcal{N}_K$. This finally leads to (5.14) in the following manner:

$$\begin{aligned}\tilde{c}_{L,K,i} &= \vartheta^i_{L,K,M}\big(\bar{c}_M - \bar{c}_K + \mathcal{O}(h^2)\big) + \vartheta^i_{L,K,N}\big(\bar{c}_N - \bar{c}_K + \mathcal{O}(h^2)\big) + \mathcal{O}(h^2)\\ &= \vartheta^i_{L,K,M}\Delta_{K,M} + \vartheta^i_{L,K,N}\Delta_{K,N} + \mathcal{O}(h^2).\end{aligned}$$

Acknowledgment. We are grateful for valuable inputs from two anonymous reviewers, whose suggestions led to a number of improvements with respect to the initial version of this manuscript.

REFERENCES

[1] Adimurthi, J. Jaffré, and G. D. Veerappa Gowda, *Godunov-type methods for conservation laws with a flux function discontinuous in space*, SIAM J. Numer. Anal., 42 (2004), pp. 179–208.

[2] Adimurthi, G. D. Veerappa Gowda, and J. Jaffré, *The DFLU flux for systems of conservation laws*, J. Comput. Appl. Math., 247 (2013), pp. 102–123.

[3] J. W. Barrett and P. Knabner, *Finite element approximation of the transport of reactive solutes in porous media. Part* II: *Error estimates for equilibrium adsorption processes*, SIAM J. Numer. Anal., 34 (1997), pp. 455–479.

[4] L. Bergamaschi, S. Mantica, and G. Manzini, *A mixed finite element-finite volume formulation of the black-oil model*, SIAM J. Sci. Comput., 20 (1998), pp. 970–997.

[5] F. Brezzi, J. Douglas, and L. D. Marini, *Two families of mixed finite elements for second order elliptic problems*, Numer. Math., 47 (1985), pp. 217–235.

[6] H. C. Brinkman, *A calculation of the viscous force exerted by a flowing fluid on a dense swarm of particles*, J. Appl. Sci. Res., A1 (1947), pp. 27–34.

[7] R. H. Brooks and A. T. Corey, *Hydraulic properties of porous media*, Technical report, Colorado State University, Fort Collins, CO, Hydrological Paper 3, (1964).

[8] S. Buckley and M. Leverett, *Mechanism of fluid displacement in sands*, Trans. AIME, 146 (1942), pp. 107–116.

[9] R. Bürger, S. Kumar, S. K. Kenettinkara, and R. Ruiz-Baier, *Discontinuous approximation of viscous two-phase flow in heterogeneous porous media*, J. Comput. Phys., 321 (2016), pp. 126–150.

[10] R. Bürger, S. Kumar, and R. Ruiz-Baier, *Discontinuous finite volume element discretization for coupled flow–transport problems arising in models of sedimentation*, J. Comput. Phys., 299 (2015), pp. 446–471.

[11] R. Bürger, R. Ruiz-Baier, and H. Torres, *A stabilized finite volume element formulation for sedimentation-consolidation processes*, SIAM J. Sci. Comput., 34 (2012), pp. B265–B289.

[12] C. Calgaro, E. Creusé, and T. Goudon, *An hybrid finite volume-finite element method for variable density incompressible flows*, J. Comput. Phys., 227 (2008), pp. 4671–4696.

[13] B. Cockburn, S. Hou, and C.-W. Shu, *The Runge-Kutta local projection discontinuous Galerkin finite element method for conservation laws.* IV. *The multidimensional case*, Math. Comp., 54 (1990), pp. 545–581.

[14] T. Q. C. Dang, Z. Chen, T. B. N. Nguyen, and W. Bae, *Investigation of isotherm polymer adsorption in porous media*, Pet. Sci. Technol., 32 (2014), pp. 1626–1640.

[15] J. W. Demmel, J. R. Gilbert, and X. S. Li, *An asynchronous parallel supernodal algorithm for sparse Gaussian elimination*, SIAM J. Matrix Anal. Appl., 20 (1999), pp. 915–952.

[16] R. E. Ewing, R. D. Lazarov, and Y. Lin, *Finite volume element approximations of nonlocal reactive flows in porous media*, Numer. Methods Partial Differential Equations, 16 (2000), pp. 285–311.

[17] S. Gottlieb, D. I. Ketcheson, and C.-W. Shu, *High order strong stability preserving time discretizations*, J. Sci. Comput., 38 (2009), pp. 251–289.

[18] S. T. Hilden, O. Møyner, K.-A. Lie, and K. Bao, *Multiscale simulation of polymer flooding with shear effects*, Transp. Porous Media, 113 (2016), pp. 111–135.

[19] E. L. Isaacson and J. B. Temple, *Analysis of a singular hyperbolic system of conservation laws*, J. Differential Equations, 65 (1986), pp. 250–268.

[20] T. Johansen and R. Winther, *The solution of the Riemann problem for a hyperbolic system of conservation laws modeling polymer flooding*, SIAM J. Math. Anal., 19 (1988), pp. 541–566.

[21] T. Johansen and R. Winther, *The Riemann problem for multicomponent polymer flooding*, SIAM J. Math. Anal., 20 (1989), pp. 908–929.

[22] C. Klingenberg and N. H. Risebro, *Stability of a resonant system of conservation laws modeling polymer flow with gravitation*, J. Differential Equations, 170 (2001), pp. 344–380.

[23] J. Könnö and R. Stenberg, *$H(\mathrm{div})-$conforming finite elements for the Brinkman problem*, Math. Models Methods Appl. Sci., 21 (2011), pp. 2227–2248.

[24] J. Kou and S. Sun, *On iterative IMPES formulation for two-phase flow with capillarity in heterogeneous porous media*, Int. J. Numer. Anal. Model. Ser. B, 1 (2004), pp. 20–40.

[25] S. Kumar, *Mixed and discontinuous Galerkin finite volume element method for incompressible miscible displacement problems in porous media*, Numer. Methods Partial Differential Equations, 28 (2012), pp. 1354–1381.

[26] S. Mishra and J. Jaffré, *On the upstream mobility scheme for two-phase flow in porous media*, Comput. Geosci., 14 (2010), pp. 105–124.

[27] M. Ohlberger, *Convergence of a mixed finite element-finite volume method for the two phase flow in porous media*, East-West J. Numer. Math., 5 (1997), pp. 183–210.

[28] S. Osher and C.-W. Shu, *Efficient implementation of essentially non-oscillatory shock-capturing schemes*, J. Comput. Phys., 77 (1988), pp. 439–471.

[29] G. F. Pinder and W. G. Gray, *Essentials of Multiphase Flow and Transport in Porous Media*, Wiley, Hoboken, NJ, 2008.

[30] G. Pope, *The application of fractional flow theory to enhanced oil recovery*, Soc. Pet. Eng. J., 20 (1980), pp. 191–205.

[31] F. A. Radu, I. S. Pop, and S. Attinger, *Analysis of an Euler implicit–mixed finite element scheme for reactive solute transport in porous media*, Numer. Methods Partial Differential Equations, 26 (2010), pp. 320–344.

[32] F. A. Radu, J. M. Nordbotten, I. S. Pop, and K. Kumar, *A robust linearization scheme for finite volume based discretizations for simulation of two-phase flow in porous media*, J. Comput. Appl. Math., 289 (2015), pp. 134–141.

[33] F. A. Radu, K. Kumar, I. S. Pop, and J. M. Nordbotten, *A robust, mass conservative scheme for two-phase flow in porous media including Hölder continuous nonlinearities*, IMA J. Numer. Anal., to appear.

[34] H.-K. Rhee, R. Aris, and N. R. Amundson, *First-Order Partial Differential Equations. Vol.* 2: *Theory and Application of Hyperbolic Systems of Quasilinear Equations*, Prentice Hall, Englewood Cliffs, NJ, 1989.

[35] D. Rodriguez, L. Romero-Zerón, and B. Wei, *Oil displacement mechanisms of viscoelastic polymers in enhanced oil recovery (EOR): A review*, J. Pet. Explor. Prod. Technol., 4 (2014), pp. 113–121.

[36] R. Ruiz-Baier and I. Lunati, *Mixed finite element–discontinuous finite volume element discretization of a general class of multicontinuum models*, J. Comput. Phys., 322 (2016), pp. 666–688.

[37] R. Ruiz-Baier and H. Torres, *Numerical solution of a multidimensional sedimentation problem using finite volume-element methods*, Appl. Numer. Math., 95 (2015), pp. 280–291.

[38] K. S. Schmid, S. Geiger, and K. S. Sorbie, *Higher order FE–FV method on unstructured grids for transport and two-phase flow with variable viscosity in heterogeneous porous media*, J. Comput. Phys., 241 (2013), pp. 416–444.

[39] K. Sudarshan Kumar, C. Praveen, and G. D. Veerappa Gowda, *A finite volume method for a two-phase multicomponent polymer flooding*, J. Comput. Phys., 275 (2014), pp. 667–695.

[40] J. P. Whiteley, *A discontinuous Galerkin finite element method for multiphase viscous flow*, SIAM J. Sci. Comput., 37 (2015), pp. B591–B612.